An Inherent Difference Between Serine and Threonine Phosphorylation: Phosphothreonine Strongly Prefers a Highly Ordered, Compact, Cyclic Conformation

Anil K. Pandey[1‡], Himal K. Ganguly[1‡], Sudipta Kumar Sinha[1,2], Kelly E. Daniels[1], Glenn P. A. Yap[1]*, Sandeep Patel[1]*, and Neal J. Zondlo[1]*

[1] Department of Chemistry and Biochemistry, University of Delaware, Newark, DE 19716, United States

[2] Department of Chemistry, Indian Institute of Technology Ropar, Nangal Road 140001 India.

* To whom correspondence should be addressed. email: *zondlo@udel.edu*, phone: +1-302-831-0197; *sapatel@udel.edu*, phone: +1-302-831-6024; *gpyap@udel.edu,* phone: +1-302-831-4441.

‡ These authors contributed equally.

Abstract

Phosphorylation and dephosphorylation of proteins by kinases and phosphatases are central to cellular responses and function. The structural effects of serine and threonine phosphorylation were examined in peptides and in proteins, by circular dichroism, NMR spectroscopy, bioinformatics analysis of the PDB, small-molecule X-ray crystallography, and computational investigations. Phosphorylation of both serine and threonine residues induces substantial conformational restriction in their physiologically more important dianionic forms. Threonine exhibits a particularly strong disorder-to-order transition upon phosphorylation, with dianionic phosphothreonine preferentially adopting a cyclic conformation with restricted ϕ ($\phi \sim$ –60°) stabilized by three noncovalent interactions: a strong intraresidue phosphate-amide hydrogen bond, an n→π* interaction between consecutive carbonyls, and an n→σ* interaction between the phosphate Oγ lone pair and the antibonding orbital of C–Hβ that restricts the χ_2 side chain conformation. Proline is unique among the canonical amino acids for its covalent cyclization on the backbone. Phosphothreonine can mimic proline's backbone cyclization via noncovalent interactions. The preferred torsions of dianionic phosphothreonine are ϕ,ψ = polyproline II helix > α-helix ($\phi \sim$ –60°); $\chi_1 = g^-$; $\chi_2 \sim$ +115° (eclipsed C–H/O–P bonds). This structural signature is observed in diverse proteins, including in the activation loops of protein kinases and in protein-protein interactions. In total, these results suggest a structural basis for the differential use and evolution of threonine versus serine phosphorylation sites in proteins, with serine phosphorylation typically inducing smaller, rheostat-like changes, versus threonine phosphorylation promoting larger, step function-like switches, in proteins.

Introduction

Phosphorylation of serine (Ser), threonine (Thr), and tyrosine (Tyr) hydroxyl groups in proteins is a predominant mechanism of intracellular signal transduction and of achieving intracellular responses to extracellular signals.[1] Over 90% of phosphorylated residues identified via phosphoproteomics are phosphoserine (pSer) or phosphothreonine (pThr) residues (Figure 1)[2], with the significant majority of these phosphorylation sites being pSer residues.[3] The preference of phosphorylation on Ser over Thr is observed in most proteins, via biases at the substrate level both of kinases (faster phosphorylation of Ser than Thr) and phosphatases (faster dephosphorylation at Thr than Ser). These general substrate preferences combine to result in a significantly higher fraction of pSer than pThr residues in cells and *in vivo*. In contrast to the general preference for phosphorylation at Ser, some kinases, phosphatases, and protein-interaction domains alternatively have a strong preference for interaction with Thr over Ser.[4-11] In addition, Thr and Ser phosphorylation sites exhibit different rates of evolutionary change, suggesting functional differences in phosphorylation at each residue.[3,12]

Ser and Thr phosphorylation induce protein-protein interactions that involve specific recognition of proteins with pSer or pThr.[5,6,13-16] However, pSer and pThr are also capable of directly interacting with the local protein backbone, and thus can directly impact local structure.[17-26] In their unmodified forms, Ser/Thr free hydroxyls can interact via hydrogen bonding with intraresidue or adjacent amide hydrogens and carbonyls, via their hydroxyl hydrogen bond donor (O–H) and/or acceptors (lone pairs). These interactions lead to significant conformational heterogeneity in Ser and Thr.[27] In contrast, pSer and pThr only exhibit hydrogen bond acceptors in the dianionic form that dominates at physiological pH (typical pK_a ~ 6),[17,20,22] suggesting the possibility of changes in backbone interactions due to phosphorylation.

In model peptides, phosphorylation strongly induces α-helix at the N-terminus of an α-helix.[26,28-30] In contrast, phosphorylation strongly disrupts α-helix in the interior of the α-helix, including complete disruption of the α-helix in a manner comparable to proline.[26,31,32] In tau-derived and model proline-rich and intrinsically disordered peptides examined previously, circular dichroism (CD) and NMR data indicated substantial conformational restriction in the dianionic phosphorylated residue compared to the unmodified or monoanionic phosphorylated residue.[24-26] Strikingly, these data also demonstrated substantially greater conformational changes due to Thr phosphorylation compared to Ser phosphorylation. Thr, as a β-branched amino acid, generally prefers a relatively more extended conformation,[33,34] although via its hydroxyl it can also function as an N-cap to stabilize α-helices.[35-37] Thus, like all encoded amino acids, Thr has inherent conformational disorder. In contrast, dianionic pThr was observed in these peptides to have a structural signature indicating a highly ordered, compact conformation, including ordered ϕ and an intraresidue phosphate-amide hydrogen bond.

Collectively, the data in tau-derived peptides, and in proline-rich and α-helical model peptides, suggest that pThr induces greater conformational restriction than pSer and induces a greater total structural change as a result of phosphorylation. Given the significance of Ser/Thr phosphorylation in intracellular signaling, we sought to more broadly examine the structural effects of Ser versus Thr phosphorylation. Ser-Pro and Thr-Pro sequences are phosphorylated by proline-directed kinases, such mitogen-activated protein (MAP) kinases and cyclin-dependent protein kinases (cdks), which are critical in signal transduction pathways and control of cell cycle progression. In total, proteomics data indicate that over 25% of Ser/Thr phosphorylated protein sites are pSer-Pro or pThr-Pro sites.[3] The identification of differences in induced

structure for pSer versus pThr at proline-directed phosphorylation sites thus would have broad implications in structural and cellular biology.

Results

In order to more broadly examine the structural effects of Ser/Thr phosphorylation, a series of peptides derived from proteins important in intracellular signaling and transcription was synthesized (Figure 2a). In addition, peptides containing a simple Ser/Thr-Pro dipeptide sequence were examined (Figure 2b), in order to identify the inherent effects of phosphorylation on structure in minimal contexts and to determine if the structural changes observed in larger peptides are also found in these minimal proline-directed kinase substrate sequences. These sequences, in combination with those examined previously (Figure 2c), represent a wide array of biomedically important proteins containing Ser/Thr-Pro sequences as well as diverse sequence contexts in the residues prior to the phosphorylated residue (acidic, basic, hydrophobic, proline, neutral polar, neutral small nonpolar).

Effects of Ser and Thr phosphorylation by CD spectroscopy. All peptides were examined by CD in the non-phosphorylated and phosphorylated forms. Ser and Thr have low polyproline II helix (PPII) propensities.[38-40] In contrast, across all peptides containing pSer-Pro or pThr-Pro sequences, phosphorylation was observed by CD to result in an increase in PPII, which is indicated by an increase in the magnitude of the positive band at ~228 nm (Figure 2e-i).[38,39,41] These results are consistent with those observed previously in tau-derived peptides and model peptides.[25] The association of this band with PPII was further confirmed by analysis of a subset of the peptides in 4 M or 8 M urea, which increases PPII[42,43] and which led to further increases in PPII for the phosphorylated peptides compared to the non-phosphorylated peptides (Figures S12-

S13). The specificity of this CD signal for PPII was also confirmed by thermal denaturation experiments, which exhibited an isodichroic point as well as both a decrease in $[\theta]_{228}$ and an increase in λ_{max} with increasing temperature, as expected for the PPII conformation melting to a random coil conformation at higher temperature (Figure S8).[38,39]

The effects of phosphorylation were also examined in Ac-Ser-Pro-OMe and Ac-Thr-Pro-OMe dipeptides (Figure 2lm). The effect of "pseudo-phosphorylation" (change of a phosphorylatable Ser/Thr to the phosphorylation mimics [phosphomimetics, phosphomimics] Asp or Glu) was also examined, using the peptides Ac-Asp-Pro-OMe and Ac-Glu-Pro-OMe (Figure 2jk).[44,45] The CD spectrum of the non-phosphorylated Thr-containing peptide exhibited an intense negative band λ_{min} = 219 nm (Figure 2m), consistent with extended and/or turn conformations that is expected for the β-branched residue Thr. The CD spectrum with Ser was less well-defined and was consistent with substantial disorder (Figure 2l). In contrast, both phosphorylated peptides when in the dianionic state exhibited an increased PPII structural signature (more positive signal at 210-220 nm)[41] and a significant change in structure from the non-phosphorylated peptides. These results indicate that induction of order is an inherent property of phosphorylation at Ser/Thr-Pro sequences. Notably, the monoanionic phosphorylated peptides exhibited only modest changes compared to non-phosphorylated Ser or Thr, indicating that the structural effects of phosphorylation are primarily mediated via the dianionic ionization state.[25] In addition, the CD spectra of peptides with Asp or Glu exhibited evidence of PPII in their anionic forms, but not their neutral forms, with greater PPII structure for Asp^- than Glu^- (Figure 2jk).

Across these peptides, Thr phosphorylation both induced a more robust PPII structure and a more dramatic overall change in structure upon phosphorylation, with stronger CD

signatures in both the non-phosphorylated and phosphorylated states. These data indicate a greater disorder-to-order (or, alternatively, an ordered-extended to ordered-PPII) change in structure upon Thr phosphorylation than upon Ser phosphorylation.

Effects of Ser and Thr phosphorylation by NMR spectroscopy. To identify residue-specific structural changes upon phosphorylation, all peptides were examined by ^{1}H NMR spectroscopy, comparing the effects of phosphorylation on Ser versus Thr residues on chemical shift (δ) and on the ϕ backbone torsion angle (via $^{3}J_{\alpha N}$, the coupling constant between H^N and Hα, and a parametrized Karplus relationship[46]) (Figure 3). In addition to peptides analyzed above by CD, peptides were also examined to compare Ser versus Thr phosphorylation in alternative local sequence contexts, including a "backbone-only" context lacking side chains beyond the β carbon on adjacent residues (Ac-A(S/T)PA-NH_2) and a context with hydrophobic residues adjacent to the phosphorylation site (Ac-L(S/T)PV-NH_2; these latter sequences are found as phosphorylated sites in the transcription factor Elk-1, the proto-oncogene transcription factor Ets-1, the RNA-splicing regulatory protein AHNAK (12 LSPV phosphorylation sites), and numerous other proteins).

Across all peptides, phosphorylation resulted in a large downfield change in the δ of the pSer/pThr amide hydrogens (H^N), as well as a reduction in $^{3}J_{\alpha N}$ (summary: Figure 3c, Table 1). These data indicate a significant increase in order and the adoption of a more compact conformation at the ϕ torsion angle upon phosphorylation (Thr average $\phi = -84^\circ$, pThr average $\phi = -55^\circ$; Ser average $\phi = -80^\circ$, pSer average $\phi = -71^\circ$). $^{3}J_{\alpha N}$ values between 6-8 Hz are typical for disorder and can result from significant conformational averaging. In contrast, $^{3}J_{\alpha N} < 6$ Hz have

unique solutions when $-165^\circ < \phi < -30^\circ$ (i.e. in the allowed region of the left half of the Ramachandran plot), and thus require a compact ϕ as the major conformation, with smaller values indicating greater order and more compact conformations in ϕ (Figure 4). The downfield H^N δ, as well as the observation of these H^N by NMR at pH 7.5-8.0 (conditions in which amide hydrogens in disordered proteins usually exchange rapidly), indicate amide protection and suggest a close interaction with the phosphate via a hydrogen bond, as has been proposed previously.[17-22,24,25,47-49]

Notably, the structural signatures observed by NMR in diverse protein-derived peptides were similarly observed in Ac-pSer-Pro-OMe and Ac-pThr-Pro-OMe (Figure 5), suggesting that minimal peptides provide a general insight into the inherent effects of proline-directed phosphorylation. At all Ser/Thr-Pro sites, the induced structures at pThr were more defined, more compact, and more ordered than the induced structures at pSer, as indicated by more downfield H^N δ and smaller $^3J_{\alpha N}$.[46] This differentiation is exemplified by analysis of Ser versus Thr phosphorylation in identical sequence contexts, including comparison of the closely related c-jun (one pThr, one pSer) and JunD (two pSer) peptides; Ac-pSer-P-OMe versus Ac-pThr-P-OMe; A(S/T)PA and L(S/T)PV tetrapeptides; and K(S/T)PP and GPP(S/T)PPGY peptides examined previously (Figure 3c). In all cases, clear differentiation is observed between the effects of pSer and pThr on structure.

The magnitude of the structural effects of phosphorylation was strongly dependent on the dianionic form of pThr: monoanionic pThr and monoanionic pSer (data at pH 4) had only modest structural effects compared to the unmodified peptides, including small downfield changes in amide δ and small decreases in $^3J_{\alpha N}$.[22] Indeed, $^3J_{\alpha N}$ for monoanionic pSer and pThr

are closer to those of the pseudo-phosphorylation mimics Asp or Glu in model peptides (Figure 5, Figure 6).

Ac-pThr-Pro-OMe was examined by NMR as a function of pH (Figure 7a). These data confirmed that the large downfield change in H^N chemical shift in pThr and the small $^3J_{\alpha N}$ observed in peptides were present only in the dianionic form of pThr, which dominates at physiological pH (p*K*a of this peptide 6.25 ± 0.07).[17,20,22] In addition to this indirect evidence suggesting an intraresidue phosphate-amide hydrogen bond in dianionic pThr, direct evidence of a hydrogen bond was indicated by a very small pThr H^N δ temperature dependence in Ac-pThr-Pro-OMe ($-\Delta\delta/T$ = 2.3 ppb/K), with $-\Delta\delta/T$ < 5 ppb considered consistent with a hydrogen bond (Figure 7bc).[50]

Additional analysis was conducted via ^1H-^{15}N HSQC and ^1H-^{13}C HSQC experiments, which provide residue-specific ^{15}N and ^{13}C δ. ^1H-^{15}N HSQC experiments (Figure 8) indicated large downfield changes in both ^1H and ^{15}N amide δ for dianionic pThr compared to either Thr or monoanionic pThr. In contrast, substantially smaller δ changes were observed for dianionic pSer compared to either Ser or monoanionic pSer (summary: Figure 8k, Table 1). These results indicate a large change in the electronic environment around pThr amide N and H atoms, consistent with a strong phosphate-amide hydrogen bond present in dianionic pThr.

In contrast, ^{13}C δ are more sensitive to conformation and less sensitive to local electrostatic environment than ^1H δ. In particular, $^1H\alpha$ and $^{13}C\alpha$ δ correlate to protein secondary structure, as is employed in Chemical Shift Index (CSI) analysis.[51-53] A subset of peptides was analyzed using ^1H-^{13}C HSQC experiments (Figure 9). The data indicated substantial upfield $^1H\alpha$ and downfield $^{13}C\alpha$ changes in δ for dianionic pThr, both of which correlate with the adoption of

more compact structure at dianionic pThr (summary: Figure 9efg, Table 1). In contrast, dianionic pSer exhibited small *downfield* ^{1}Hα and small *upfield* ^{13}Cα changes in δ, differing both in the sign and the magnitude of the changes compared to those in pThr.

We previously observed[25] that the activation loop pThr197 of protein kinase A (PKA) (pdb 1rdq,[54] 1.26 Å, local sequence RTW**pT**LCG) exhibited a structure similar to that which we found in tau-derived proline-rich peptides, including PPII ϕ,ψ torsion angles, a hydrogen bond to its own amide hydrogen, a g^- conformation in χ_1, and, surprisingly, an eclipsed C–Hβ/Oγ–P bond ($\chi_2 \sim +120^\circ$). The CD and NMR spectra of pThr and, to a lesser extent, pSer in peptides herein were consistent with this main chain conformation observed crystallographically in PKA. To identify the side-chain conformational changes upon phosphorylation, selected peptides were analyzed by NMR (Figure 10) to determine the coupling constants $^{3}J_{\alpha\beta}$ (Figure 10a and Supporting Information) and $^{3}J_{\mathrm{PH}\beta}$ (Figure 10b). $^{3}J_{\alpha\beta}$ reports on the χ_1 torsion angle, in which a maximum value of ~10 Hz indicates an *anti*-periplanar relationship of Hα and Hβ, and thus a g^- conformation, via a parametrized Karplus relationship.[55,56] $^{3}J_{\mathrm{PH}\beta}$, correlates to the χ_2 torsion angle (local maximum of 10.5 Hz at $\chi_2 \sim +120^\circ$ with an eclipsed/*syn*-periplanar relationship of the Oγ–P and C–Hβ bonds).[57] Across all peptides examined, the $^{3}J_{\alpha\beta}$ coupling constants increased upon Thr phosphorylation (Thr mean $^{3}J_{\alpha\beta}$ = 6.4 Hz, pThr mean $^{3}J_{\alpha\beta}$ = 9.2 Hz, data from 4 peptides) (Figure 10a). In pThr residues, both $^{3}J_{\alpha\beta}$ and $^{3}J_{\mathrm{PH}\beta}$ (mean pThr $^{3}J_{\mathrm{PH}\beta}$ = 8.8 Hz) approached the maxima expected if the crystallographically observed conformations were the only conformation present in these peptides (Figure 10ab), a surprising result given the inherent disorder expected

in short peptides. In contrast, the $^{3}J_{PH\beta}$ values for the diastereotopic pSer Hβ were smaller (mean pSer $^{3}J_{PH\beta}$ = 5.9 Hz) and not distinct in any condition examined, consistent with greater χ_2 conformational hetereogeneity in pSer (Figure 10b).

In addition, we observed an 8–9 Hz reduction in $^{1}J_{C-H\beta}$ in dianionic pThr compared to Thr or monoanionic pThr (Figure 10c), consistent with greater ordering in χ_2 in dianionic pThr. The chemical interpretation of these data will be discussed below. We also observed an increase in $K_{trans/cis}$ (decreased population of *cis* amide bond) for peptides with dianionic pThr, compared to non-phosphorylated Ser or Thr, to either monoanionic pSer or pThr, or to dianionic pSer (Figure 10d), suggesting a stronger n→π^* interaction stabilizing the *trans* amide bond in dianionic pThr.[58] Consistent with this interpretation, a substantial downfield change was observed at the pThr carbonyl ^{13}C δ. In total, all lines of evidence by NMR spectroscopy indicate large changes in structure and large increases in order when going from Thr to dianionic pThr (summary: Figure 10e and Table 1), compared to the changes from Ser to pSer.

Analysis of pThr and pSer in the Protein Data Bank (PDB). The results above, combined with prior work, suggest that structural changes induced by phosphorylation on Ser and Thr are general, with a particularly strong conformational bias in dianionic pThr. To examine this generality, pSer and pThr residues in the PDB were examined, and the conformational preferences of these phosphorylated residues compared to non-phosphorylated Ser and Thr from high-resolution structures (≤ 1.25 Å resolution, ≤ 25% sequence identity). Due to a limited number of pSer and pThr residues in the PDB, which is a caveat to this analysis, phosphorylated proteins were examined with expanded resolution (≤ 2.50 Å) and sequence identity (95%)

cutoffs, yielding 234 pSer and 155 pThr residues that were analyzed, including residues in globular proteins and ligands in protein-protein complexes (Tables S1, S2).

These data indicate a remarkable degree of order at pThr residues, compared to non-phosphorylated Thr or Ser, or to pSer (Figure 11). The Ramachandran plot of pThr exhibits a strong preference for highly ordered values of ϕ, with PPII the major conformation and α-helix a minor conformation. For pThr, relatively few structures are observed in either the δ or β regions of the Ramachandran plot, and no structures are observed on the right side of the Ramachandran plot. These data are consistent with the conformational preferences observed herein and previously in diverse sequence contexts, where pThr exhibited a small $^3J_{\alpha N}$ indicative of a high degree of order in ϕ consistent with either PPII or α-helix. In contrast, Thr more frequently adopts a more extended and/or more disordered conformation due to β-branching of the sidechain and the possibility of multiple sidechain-main chain hydrogen bonds.

pSer residues in the PDB exhibit greater order than Ser, with similar but less distinct preferences for PPII and α-helix as pThr, and weaker overall conformational preferences than pThr. The conformational effects of Thr versus Ser phosphorylation were particularly notable when examining the ϕ, χ_1, and χ_2 torsion angles individually. pThr exhibits a strong preference for $\phi \sim -60^\circ$, in contrast to the more extended ϕ preference of Thr and the more diffuse ϕ preference of pSer. pThr also exhibits a strong χ_1 preference for the g^- conformation, in contrast to the similar g^- and g^+ preferences of Thr, and the absence of a significant χ_1 preference for Ser or pSer.[27]

Similarly, pThr strongly prefers $\chi_2 \sim +120^\circ$, with eclipsing or near-eclipsing Oγ–P and C–Hβ bonds. Interestingly, eclipsing Oγ–P and C–Hβ bonds are also observed ($\chi_2 \sim +120^\circ$ or –

120°) as minor conformations of pSer, indicating that the eclipsed conformation is energetically favorable. However, for pSer the sterically preferred fully extended $\chi_2 \sim 180°$ is the major conformation. The low population of conformations with negative values of χ_2 is not surprising for pThr, as these conformations would induce significant steric repulsion between the large phosphate group and the γ-CH_3 group and/or the protein main chain. The apparent preference for an eclipsed conformation was not expected for pThr, although a similar interaction has been observed by NMR in glycosylated Thr.[59-61] The greater length of the O–P bond (1.62 Å) compared to the C–H bond (1.09 Å) is expected to reduce, but not eliminate, the steric cost of an eclipsing interaction (H•••P distances of 2.5–2.6 Å were observed, which are substantially less than the 3.0 Å sum of the van der Waals radii of P and H).

Further analysis indicates a Cβ–Oγ–P bond angle of ~120° in these structures (i.e. sp^2-type geometry at Oγ). Thus, the sp^2-like O lone pair and the Cβ-Hβ bond lie within the same plane, with the Oγ sp^2-like lone pair and the σ* of C–Hβ aligned for potential orbital overlap and electron delocalization. The unusual conformational preference for an eclipsed conformation of χ_2 is herein ascribed to the presence of a favorable n→σ* hyperconjugative interaction between the coplanar sp^2-like Oγ lone pair (n) of the electron-rich dianionic pThr and the antibonding orbital (σ*) of the electron-deficient C–Hβ bond. This type of n→σ* interaction (known as the Perlin effect) is observed at H–C–O–**:** torsion angles in carbohydrates when the C–H is axial, and thus *anti*-periplanar to the oxygen lone pair, and therefore the oxygen lone pair is *syn*-periplanar with the C–H σ*, as is observed herein.[62-64] In these stereoelectronic effects, the 1-bond C–H coupling constant $^1J_{CH}$ is observed to be 8-10 Hz smaller than in similar C–H bonds that are not stabilized by this interaction. Indeed, consistent with this interpretation, $^1J_{C^\beta H^\beta} = 138$

Hz for dianionic pThr in Ac-pTP-OMe, compared to $^{1}J_{C^{\beta}H^{\beta}}$ = 147 Hz in non-phosphorylated Ac-TP-OMe and $^{1}J_{C^{\beta}H^{\beta}}$ = 148 Hz in monoanionic Ac-pTP-OMe (Figure 10c), similar to a typical Perlin effect. These data indicate that a significant interaction only occurs when pThr is in the more electron-rich dianionic state, where the O lone pair can function as an effective lone pair electron donor. Collectively, these results suggest that stabilization of the χ_2 eclipsed conformation occurs via an n→σ* stereoelectronic effect.

pThr exhibited a particularly strong preference for an *intraresidue* hydrogen bond between the phosphate and the pThr amide hydrogen (Figure 11). In contrast, pSer had a substantially lower preference than pThr for an intraresidue phosphate-amide hydrogen bond, consistent with the frequency of pSer adopting the sterically preferred fully extended χ_2. The PDB data are consistent with the observations herein of more downfield H^N and N^H amide δ and slower amide exchange at pH 7.5-8.0 (as evidenced by narrower linewidths/less broadening) for pThr amides compared to pSer amides in peptides.

n→π* interactions between adjacent carbonyls are a significant force stabilizing local interactions between consecutive residues.[58,65-70] n→π* interactions involve electron delocalization via orbital overlap between the lone pair of a donor carbonyl oxygen (n refers to the lone pair, on the *i* residue) and the antibonding (π*) orbital of the subsequent carbonyl (*i*+1 residue). An n→π* interaction can be identified by an O_i•••C_{i+1} interresidue distance that is less than the sum of the C and O van der Waals radii (d < 3.22 Å, with shorter distances indicating greater orbital overlap/greater electron delocalization) and an O_i•••C_{i+1}=O angle ~109°, that maximizes orbital overlap. Data from the PDB indicate a strong preference for pThr residues to exhibit n→π* interactions between the carbonyl prior to pThr (i.e. the carbonyl directly

conjugated to the pThr amide N–H) and the pThr carbonyl (Figure 12). The net effect of this interaction is to induce strong local ordering of two consecutive carbonyls.

Analysis of pSer residues indicated a relatively reduced likelihood of n→π* interactions and less clustering around the ideal 109° angle for n→π* interactions. Notably, across all residues, there was a strong correlation of O•••C interresidue distance with the ϕ torsion angle, consistent with n→π* interactions being more favorable in more compact conformations.[66,67] NMR data on Ac-pTP-OMe and KpTPP peptides were also consistent with an n→π* interaction stabilizing structure, with significant changes in the acetyl and pThr carbonyl ^{13}C δ in the phosphorylated peptides compared to the non-phosphorylated peptides (Figure 10d). Interestingly, in Ac-pTP-OMe, as well as in tetrapeptides with TP sequences, phosphorylation also induced a significant increase in preference for *trans* over *cis* amide bonds when pThr was dianionic (Figure 10d). In contrast, in Ac-pSP-OMe and other peptides with dianionic pSer, an increase in the population of *cis*-proline was observed compared to the unmodified Ser. These data suggest an inherent difference in the propensity of pSer and pThr to promote a *cis* amide bond.[71] The increased preference for a *trans* amide bond with pThr could potentially be due to the enhanced n→π* interaction in the phosphorylated peptide, whereby the intraresidue hydrogen bond makes the conjugated carbonyl more electron-rich (more δ^-), and therefore a better electron donor for an n→π* interaction.

X-ray crystallography of a phosphothreonine-proline dipeptide. The structural signatures observed for pThr in the PDB were consistent with NMR data in minimal Ac-pTP-OMe dipeptides. To further examine the structural effects of Thr phosphorylation, a derivative of this peptide was synthesized with an iodobenzoyl acyl group (4-I-Bz-pThr-Pro-NH_2) and a C-terminal amide. This peptide was independently synthesized in both the L-peptide and D-peptide

enantiomeric forms, to allow for an enhanced possibility of crystal formation via racemic crystallization.[72] NMR data indicated that the peptide was conformationally similar to Ac-pThr-Pro-OMe (downfield pThr H^N δ, small pThr $^3J_{\alpha N}$, downfield pThr Hα, upfield pThr Cα δ, and a reduced $^1J_{CH\beta}$ in the dianionic form; see the Supporting Information for details).

Both the single-enantiomer (L-peptide) and the racemic (1:1 mixture of L-peptide and D-peptide) solutions of 4-I-Bz-pThr-Pro-NH_2 crystallized via vapor diffusion. The single-enantiomer crystal structure was solved at 0.80 Å resolution (Figure 13).[73] The racemic crystal structure was solved at 0.87 Å resolution, with two non-equivalent molecules in the asymmetric unit. The crystal structures recapitulated all of the structural features identified via NMR spectroscopy across diverse peptide sequences and via bioinformatics analysis. In all three independent molecules across the two crystal structures, pThr adopted a PPII conformation with a compact value of ϕ, a close intraresidue phosphate-amide hydrogen bond, a close intercarbonyl O_{Ac}•••C_{pThr}=O distance, a g^- χ_1 conformation, and an eclipsed χ_2 conformation (Figure 13d). Interestingly, in the single-enantiomer structure, a water molecule was localized by hydrogen bonding between the amide-interacting phosphate oxygen and the pThr carbonyl. Hydrogen bonding at the acceptor carbonyl enhances the interaction strength of an n→π* interaction.[74] The bound water observed herein could potentially be an additional factor by which solvation associated with Thr phosphorylation stabilizes the PPII conformation.

The strong intraresidue hydrogen bond for dianionic pThr observed crystallographically results in a *non-covalently* cyclic structure of pThr, analogous to the *covalently* cyclic structure of proline (Figure 13g). Consistent with this interpretation, we previously observed that dianionic pThr is strongly destabilizing to α-helices when located at the center and C-terminus of an α-helical sequence, in a manner comparable to the effects of Pro on α-helices.[26,31] The

crystallographic data also indicate an n→π* interaction between the iodobenzoyl carbonyl and the pThr carbonyl. An n→π* interaction is further observed between the pThr carbonyl and the Pro carbonyl, with the Pro exhibiting an *exo* ring pucker and PPII conformation. These data indicate the ability of Thr phosphorylation to organize multiple consecutive residues. Notably, these non-covalent interactions are expected to be synergistic in leading to an ordered structure: a phosphate-amide hydrogen bond would be expected to increase electron density on its conjugated carbonyl, making it a better electron donor for an n→π* interaction with the subsequent carbonyl (Figure 10d).[69]

These data represent the first small-molecule X-ray crystal structure of a peptide containing pThr. The X-ray structure of a simple pThr-containing peptide indicates that dianionic pThr has strong inherent conformational preferences that are manifested in a side chain-main chain intraresidue hydrogen bond, restrained ϕ, ψ, χ_1, and χ_2 torsion angles, and a favorable interresidue n→π* interaction that organizes consecutive residues. Moreover, these data suggest that the conformational preferences observed for pThr residues in the PDB, in diverse sequence contexts, reflect the strong inherent residue preferences of dianionic pThr.

Computational investigations on minimal peptides containing pThr. To further characterize the molecular basis of the highly stabilized structure of pThr within peptide and protein contexts, calculations were conducted by density functional theory (DFT) methods on a minimal Ac-pThr-NMe_2 structure, on pThr-Pro dipeptides, on variants of these with the bridging water molecule observed in the single-enantiomer crystal structure, and on the equivalent peptides with pSer in place of pThr. In addition, calculations were conducted on Ac-pThr-NMe_2 and Ac-pThr-Pro-NMe_2 molecules that include 7 water molecules initially derived from the single-enantiomer crystal structure, and on Ac-pThr-Pro-NH_2 that included 8 water molecules as

well as the K^+ and Na^+ ions from this crystal structure. These calculations were conducted in order to examine the effects of implicit versus explicit solvation on the overall structure and on the non-covalent interactions.

Geometry optimization calculations yielded structures (Figure 14, Table 2) that were similar to those observed crystallographically and to the conformational features observed in solution by NMR spectroscopy. In particular, across all peptides examined, the resultant structures exhibited ϕ and ψ torsion angles and other conformational features that were very similar to those observed crystallographically. In addition, the data indicated significant pyramidalization at the pThr carbonyl (2.2–3.0°), but not at the acetyl carbonyl (≤ 0.3°). This pyramidalization is consistent with an important role of the n→π* interaction in pThr stabilizing the PPII conformation, whereby the acceptor carbonyl exhibits partial pyramidalization analogous to the early stages of a nucleophilic attack of one carbonyl on the other.[58,65,67,70] Interestingly, equivalent geometry-optimized structures with pSer exhibited somewhat more extended conformations and longer n→π* interaction distances, even with the same overall conformational features, consistent with the reduced driving force for a compact conformation for pSer compared to pThr. In addition, when pSer had a *trans* conformation at χ_2, which is the major χ_2 conformation in the PDB, the pyramidalization at the pSer C=O was greatly reduced compared to when pSer had a χ_2 conformation (~ +110°) similar to that observed in dianionic pThr. These results suggest that an *intraresidue* phosphate-amide hydrogen bond increases the strength of the *interresidue* n→π* interaction, via an increase in the electron density at the electron-donor carbonyl.

Natural bond orbital (NBO)[75] analysis was conducted on Ac-pThr-NMe_2 (Figure 14b-d). Structural analysis revealed strong orbital overlap between the nonbonding phosphate oxygen

lone pair and the amide N–H σ* in the phosphate-amide hydrogen bond, as expected. Similarly, the donor (*i*–1) carbonyl and the acceptor pThr carbonyl (*i*) exhibited strong orbital overlap between the O_{i-1} lone pair (n) and π* of the acceptor carbonyl (Figure 14c), as previously seen for favorable n→π* interactions.[67,76]

In addition, significant stabilization energy and orbital overlap were observed between the Oγ lone pair (n) and the antibonding orbital (σ*) of the C–Hβ bond (Figure 14d), indicating that a favorable n→σ* interaction is associated with the preference for an eclipsed conformation at χ_2. Analysis of the energetics of bond rotation about the Cβ–Oγ bond was conducted using a minimal isopropyl phosphate model of the pThr side chain (Figure 14fg). These calculations indicated that, despite unfavorable sterics, the eclipsed conformation (∠ H–C–O–P ~ 0°, which correlates to χ_2 ~ +120°) is the minimum energy conformation at the χ_2 torsion angle, consistent with this conformation being the dominant χ_2 for pThr. In addition, eclipsed conformations (∠ C–C–O–P or χ_2 ~ +120° or –120°) were also observed to be favorable minor conformations (inflection points) for an ethyl phosphate model of pSer (Figure 14hi), with the *anti* conformation (∠ C–C–O–P or χ_2 ~ 180°) the lowest in energy, consistent with bioinformatics data.

Finally, computationally optimized structures were analyzed with explicit solvation on the phosphate (Figure 14lmn), using the water molecules and ions observed in the single-enantiomer crystal structure for initial geometries. These structures had conformations that were broadly similar to those with implicit solvent. However, the structures with explicit solvation exhibited hydrogen bond lengths that were closer to those observed crystallographically. Notably, the structures with explicit solvation also exhibited χ_2 torsion angles with almost

perfectly eclipsed C–H and O–P bonds (∠ Hβ–C–O–P –1˚), indicating selection *for* the eclipsed conformation in pThr. In sum, these calculations indicate, consistent with experimental data, that dianionic pThr is a uniquely ordered amino acid.

Discussion

We have conducted a comprehensive analysis of the structural effects of Ser and Thr phosphorylation, using a combination of solution analysis of peptides by CD and NMR spectroscopies, bioinformatics analysis of pSer and pThr residues in the PDB, small molecule X-ray crystallography of a pThr-Pro dipeptide, and calculations on minimal peptides containing pThr. Across all size scales and by all methods employed, dianionic pThr was observed to be highly ordered, exhibiting a strong preference for a compact ϕ torsion angle ($\phi \sim -60^{\circ}$). This degree of ordering in ϕ is unique among all examined canonical and post-translationally modified amino acids, suggesting that dianionic pThr has defined structural roles. The ordering in dianionic pThr is supported by three non-covalent interactions (Figure 15): a strong intraresidue phosphate-amide hydrogen bond, an n→π* interaction between the carbonyls of adjacent residues that results in ordering of both residues, and an n→σ* interaction between the phosphate Oγ lone pair (n) and the σ* of the C–Hβ that restricts the conformation of χ_2. These non-covalent interactions strongly restrict the ϕ, χ_1, and χ_2 torsion angles, and provide additional strong biases to the ψ and ω torsion angles. The overall effect of this combination of interactions is a non-covalently bicyclic structure that fundamentally restricts dianionic pThr to preferentially adopt either a PPII or α-helix conformation. Notably, the non-covalently cyclic structure of dianionic pThr is analogous to the covalently cyclic structure of Pro (Figure 13g), consistent with

the similar position-dependent effects of dianionic pThr and Pro that have been observed on α-helix stability and in inducing PPII.[24-26,31]

The structural effects observed herein are dependent on the dianionic state of pThr that predominates at physiological pH. Only modest structural changes were observed for monoanionic pThr. Similarly, the (monoanionic) pseudo-phosphorylation mimics Asp and Glu were not capable of replicating all of the structural effects of dianionic pThr, exhibiting structures that were intermediate between unmodified Thr and dianionic pThr. In addition to electrostatic differences, these data provide a fundamental structural basis for the inability of pseudo-phophosphorylation mimics to fully replicate the functional effects of phosphorylation in all cases.

In contrast, the structural effects of phosphorylation at Ser were relatively more modest. While dianionic pSer *can* adopt a structure with all of the features of dianionic pThr, including an eclipsed C–H/O–P bond ($\chi_2 \sim +120^\circ$ or -120°), the absence of a γ-methyl group in pSer results in greater inherent conformational heterogeneity,[61] including a much wider range of conformations at ϕ, ψ, χ_1, and χ_2 and a substantially reduced likelihood of an intraresidue phosphate-amide hydrogen bond. In addition, as was observed with pThr, the structural effects of pSer were more modest in the monoanionic state. Moreover, the non-phosphorylated states of Ser and Thr exhibit substantially different conformational preferences, due to multiple possible side chain-main chain hydrogen bonds and the general preference for a more extended conformation for the β-branched amino acid Thr.[27,33,34] These differing inherent conformational preferences of Ser versus Thr are observable by NMR, by CD, and within the PDB.

Moreover, the greater conformational restriction at dianionic pThr compared to pSer or to either Asp or Glu suggests that pseudo-phosphorylation is more likely to be effective at Ser than

Thr phosphorylation sites. Although pseudo-phosphorylation partially or fully rescues function at Ser and Thr sites in numerous systems, it is also ineffective in many cases. The effects of phosphorylation versus pseudo-phosphorylation have been examined at the activation loop phosphorylation site Thr197 in protein kinase A (PKA).[77] Here, pseudophosphorylation results in a large loss of enzymatic activity compared to activated PKA with pThr. Notably, Thr is exceptionally conserved in PKA orthologs that are widely divergent evolutionarily (including human, mouse, elephant, pufferfish, *Xenopus*, *Drosophila*, *C. elegans*, *S. cerevisiae*, and slime molds), despite the pThr γ-methyl group being solvent-exposed in crystal structures of activated PKA. In protein kinases with active site phosphorylation, typically in the non-phosphorylated state the activation loop is disordered, with no observed electron density. In contrast, phosphorylation induces order, resulting in electron density for the entire activation loop.[78] These effects have previously been ascribed to electrostatic and hydrogen bonding interactions with Arg or Lys residues. We propose that the inherent ordering at the phosphorylation site is central to the conformational changes in active site phosphorylation, providing a structurally rigid nucleus for other longer-range interactions that further stabilize the structure of the activation loop. Moreover, we hypothesize that the inherent ordering is greater in protein kinases containing activation loop Thr phosphorylation than in activation loop Ser phosphorylation. Notably, among the human protein kinases, Thr is more common than Ser at known or predicted activation loop phosphorylation residues, despite the inherently greater frequency of Ser phosphorylation.

Ser/Thr phosphorylation and multiple-site phosphorylation functional effects have been examined in numerous contexts.[23,79-85] For example, phosphorylation of the transcription factor p53 at multiple Ser sites leads to a graded enhancement of binding to the transcriptional co-

activator CBP, with increased levels of phosphorylation enhancing protein binding and function. In contrast, Thr phosphorylation at a single site in p53 (Thr18) functions as an on-off switch in binding to the oncoprotein MDM2.[79,86] Moreover, the cystic fibrosis transmembrane conductance regulator (CFTR) regulatory region exhibits numerous (mostly Ser) phosphorylation sites that enable a graded (rheostat) response to control interactions with numerous protein targets, with maximum response dependent on multiple phosphorylation events.[87] In contrast, Thr phosphorylation at two residues of the intrinsically disordered protein 4E-BP2 functions as a regulatory switch, inducing protein folding and changing affinity to binding partners by over 1000-fold.[80] The data herein provide a context for considering the structural and functional effects of Ser versus Thr phosphorylation: Ser phosphorylation sites inherently exhibit relatively smaller structural effects, suggesting they serve a predominant role when phosphorylation requires a graded (rheostat-like) response, with full functional changes requiring multiple phosphorylation events. In contrast, Thr phosphorylation exhibits significantly more dramatic structural effects, most appropriate for large functional effects via step function-like structural switches.

Interestingly, there are a number of proteins that exhibit exceptional specificity for Thr phosphorylation. The protein kinase LKB1, associated with energy homeostasis, diabetes, and organism lifespan, specifically phosphorylates Thr residues in target proteins.[4,88] FHA domains control protein-protein interactions through the specific binding of proteins phosphorylated on Thr.[5,6] The pyruvate kinase M2, which acquires protein kinase activity when binding to small molecule regulators, is specific for phosphorylation at Thr.[7,8] In addition, the protein phosphatase cdc14 selectively (> 1000-fold specificity) dephosphorylates pSer residues, leaving pThr residues.[89] Moreover, a preference for Ser versus Thr phosphorylation is encoded in protein

kinases via the presence of a Phe (Ser-specific) versus hydrophobic aliphatic (Thr-specific) residue at the DFG+1 site.[11] Combined with the observation of differential evolution of Thr and Ser phosphorylation sites,[3] the data suggest an inherent difference in the native functional application of Ser versus Thr phosphorylation sites. These results also suggest Thr phosphorylation sites as having greater importance than Ser phosphorylation sites for induced structural effects of phosphorylation. The data herein provide a fundamental structural basis for understanding the differential application of Ser versus Thr phosphorylation within proteins.

Undoubtedly, the results described herein will be context-dependent, with certain sequence and structural contexts capable of promoting dianionic pThr structures that differ from those observed as the predominant conformation of pThr observed herein. For example, while the bioinformatics analysis included *all* pThr residues within proteins, with *any* amino acid following pThr, the peptide studies herein only included pThr-Pro sequences. Non-proline residues after pThr will likely allow greater conformational heterogeneity, especially in protein contexts rich with groups that can hydrogen bond to the pThr phosphate. Most importantly, monoanionic pThr exhibits only modest conformational preferences, suggesting that local structural contexts that promote monoanionic pThr, or that allow binding of multiple amide hydrogens to pThr, will lead to an alternative structure at pThr.[80]

pThr is a quite sterically hindered amino acid, with both a β-branch and a large phosphate group. Indeed, the steric effects of the phosphate group are observed within pSer, which is commonly observed with an extended side-chain conformation that places the sterically demanding phosphate far from the protein backbone (Figure 11, pSer, $\chi_2 \sim 180^\circ$). However, despite this steric hindrance, pThr nonetheless strongly prefers a highly compact conformation.

This result is fundamentally surprising, and indicates the inherent strength of the stereoelectronic effects driving the compact conformation observed herein for dianionic pThr.

Modeling of the effects of protein post-translational modifications is a central goal in order to deduce the complexities of the functional and dynamic proteome. Given the critical roles of protein phosphorylation in intracellular regulation, the development of appropriate force fields for the accurate modeling of the structural effects of post-translational modifications has attracted considerable interest, as well as the recognition that current force fields are insufficient for accurate modeling of the structural effects of phosphorylation.[19,21,90-95] The work herein provides important structural constraints to allow the improved modeling of the effects of protein Ser and Thr phosphorylation.

Intrinsic disorder is an inherent feature of protein phosphorylation sites, with disorder required for protein kinase recognition of substrates.[96,97] In addition, the majority of phosphorylation sites, including those in protein fragments examined herein, are in regions that remain intrinsically disordered even after phosphorylation. The extant crystallographic data in these proteins thus are dependent in part on data of protein complexes with these protein segments, which remain quite limited and could potentially be driven by coupled protein binding and folding rather than reflecting the conformational ensemble of these protein segments. The data herein suggest that Thr phosphorylation inherently induces a high degree of local order in proteins, including within intrinsically disordered regions of proteins. In contrast, Ser phosphorylation is capable of inducing a similarly ordered structure, but exhibits a significantly larger range of preferred conformations. These insights have broad potential application in understanding residual and induced structure within disordered regions of proteins.

Conclusions

We have investigated the inherent structural effects of Ser versus Thr phosphorylation. We have found, through a combination of biophysical analysis in peptides, small molecule X-ray crystallography, analysis of the PDB, and quantum calculations, that Thr phosphorylation induces a particularly strong disorder-to-order conformational change. Dianonic pThr strongly prefers a highly ordered conformation, with a compact $\phi \sim -60^\circ$; $\psi \sim -30^\circ$ or $+130^\circ$ (α-helix or PPII); and defined χ_1 ($\sim -60^\circ$) and χ_2 ($\sim +115^\circ$). Dianionic pThr has a strong preference for a non-covalently bicyclic structure stabilized by three non-covalent interactions: an intraresidue phosphate-amide hydrogen bond, an interresidue n→π* interaction organizing consecutive carbonyls, and an n→σ* interaction between the phosphate Oγ lone pair and the Cβ-Hβ σ* first described herein (Figure 15). In combination with the known general preference of non-phosphorylated Thr for a β/extended conformation (see also Figure 11), these data suggest an inherent difference between phosphorylation of Thr and phosphorylation of Ser residues in proteins, with a greater structural change on Thr phosphorylation than Ser phosphorylation. Thr phosphorylation results in more step-like changes in protein structure and function, while Ser phosphorylation results in more graded or rheostat-like structural and functional changes. These results have broad implications in the differential regulation of proteins by Thr versus Ser phosphorylation.

Experimental

Peptide synthesis. Protein-derived peptide sequences are from the indicated residues of the human protein. The peptide sequence for JunD was derived from the murine JunD. Dipeptides were synthesized by solution-phase methods. Larger peptides were synthesized by

standard Fmoc solid-phase peptide synthesis, subjected to cleavage from resin and deprotection, and purified to homogeneity via reverse-phase HPLC. Phosphorylated peptides were synthesized via trityl-protected Ser or Thr residues, selective trityl deprotection, phosphitylation with O,O'-dibenzyl,N,N-diisopropyl phosphoramidite, and oxidation with *t*-butyl hydroperoxide. Peptides were characterized for identity by mass spectrometry and NMR spectroscopy. Details of synthesis and characterization are in the Supporting Information.

Circular dichroism. CD spectra were collected on a Jasco J-810 Spectropolarimeter in a 1 mm cell in water containing 5 mM phosphate buffer (pH 8 or as indicated) and 25 mM KF at 25 ˚C unless otherwise indicated. Data on the $Plk1_L$ peptide were collected at 2 ˚C. Data represent the average of at least three independent trials. Data were background corrected but were not smoothed. Error bars are shown and indicate standard error. Tabulated data and additional CD spectra are in the Supporting Information.

NMR spectroscopy. NMR spectra were collected on a Brüker 600 MHz spectrometer with a cryoprobe or TXI probe. ^{31}P NMR data were collected on a Brüker 400 MHz spectrometer with a BBFO probe. Unless otherwise indicated, NMR experiments were conducted at 25 ˚C in 90% H_2O/10% D_2O or 100% D_2O with 5 mM phosphate buffer (pH 4 for non-phosphorylated peptides, pH 7.5 for phosphorylated peptides) and 25 mM NaCl. $^3J_{H\alpha H\beta}$ and $^3J_{PH\beta}$ coupling constants were determined in 100% D_2O to eliminate coupling to the amide hydrogen. Full experimental details, full spectra, and tabulated data are in the Supporting Information.

PDB analysis. The RCSB protein data bank (PDB) was probed for sequences with Thr, sSer, pThr (3-letter code TPO), and pSer (3-letter code SEP) residues. Ser and Thr were identified from a non-redundant database of protein structures with ≤ 25% sequence identity and ≤ 1.25 Å resolution using the PISCES server. A total of 14,943 Ser and 13,942 Thr residues were

identified.[98] The number of protein structures solved through X-ray crystallography with phosphorylated Thr and Ser is significantly lower. To increase the database size for reliable statistics, the conditions for the non-redundant sequence database were relaxed significantly to ≤ 95% overall sequence identity. These structure and sequence requirements led to the identification of 229 pThr residues from 141 pdb files and 374 pSer residues from 220 pdb files (Tables S1 and S2), which includes identical chains from an individual pdb structure. For those pdb files with multiple sequence-equivalent chains, only one chain (among the sequence-equivalent chains) was included for analysis (either the first chain in the file, or the most ordered chain if differences in order were identified) and final plots, such that it represents an unbiased analysis of phosphorylated residues from all the different protein structures without repetitive sequences. The database was finally curated by rejecting structures with > 2.5 Å resolution. For accurate representation of structural elements, any structure with missing residues immediately preceding or following a phosphorylated residue, or phosphorylated residues missing any side chain heavy atom (either due to inherent disorder or to limitations of the X-ray structure), was excluded from the analysis. This process led to the identification of 155 pThr residues and 234 pSer residues included in the final statistical plots (Figures 11 and 12). The dihedral angles were calculated using in-house programs written in the Perl programming language. Full tabulated data for the identified pThr and pSer residues are in Tables S1 and S2, respectively.

X-ray crystallography. *Racemic crystallization*. A 1:1 mixture of L- and D-peptide enantiomers of 4-iodobenzoyl-pThr-Pro-NH_2 (pH adjusted to 7.8 in water and dried) was allowed to dissolve in 1:1 MeOH:*t*-BuOH and subjected to crystallization at 25 ˚C by sitting-drop vapor diffusion using a *t*-BuOH reservoir. The racemic peptide crystallized over a period of one week. The crystals were diffracted using Cu radiation at 30 seconds per frame. Disorder in

the crystals, potentially due to the large volume occupied by water (10 water molecules localized per asymmetric unit) and sodium atoms that are expected to be relatively mobile, resulted in a maximum resolution of 0.87 Å. No symmetry higher than triclinic was observed. Refinement in the centrosymmetric space group P–1 yielded chemically reasonable and computationally stable results.[99] Two similar, yet symmetry-unique, molecules of the peptide were observed in the asymmetric unit. Only three sodium atoms can be localized per two peptides; it is likely that the fourth expected counterion resided in a highly disordered portion of the electron-density map centered near the origin (469 $Å^2$, 122 e) that could not be modeled, and that was thus treated as diffused contributions.[100]

4-Iodobenzoyl-phospho-L-*threonine*-L-*proline amide*. The single-enantiomer compound was subjected to crystallization via vapor diffusion of a solution of 50% methanol in *tert*-butanol (v/v) with *tert*-butanol at room temperature. Crystals formed over a period of two years, in the orthorhombic space group $P2_12_12_1$. The structure was solved by standard methods in X-ray crystallography, with a resultant resolution of 0.80 Å. For this crystal structure, all non-hydrogen atoms and the hydrogen atoms involved in hydrogen bonding were localized from the difference map. These structures were deposited in the Cambridge Structural Database under the depository numbers CCDC 1877191 and 1877192.

Calculations. Calculations were conducted using Gaussian09[101] on a series of models (Ac-pThr-NMe_2, Ac-pThr-NMe_2•bridging H_2O, Ac-pThr-Pro-NMe_2, Ac-pThr-Pro-NMe_2•bridging H_2O, Ac-pSer-NMe_2, Ac-pSer-NMe_2•H_2O, Ac-pSer-Pro-NMe_2) that were initially derived from crystallographically observed structures. Structures were chosen to include an acetyl group at the N-terminus, which provides an appropriate balance between computational simplicity and appropriately representing the electronic properties of the donor carbonyl in an

n→π* interaction.[102] Molecules were analyzed with a dimethyl amide on the C-terminus in order to avoid potential artefacts due to the presence of an unsatisfied hydrogen bond donor. Final geometry optimization calculations were conducted in Gaussian using the M06-2X DFT method[103] and the 6-311++G(3d,3p) basis set,[104] using implicit solvation with water via a continuum polarization model (IEFPCM).[105] All final geometry-optimized structures had zero imaginary frequencies.

The single-enantiomer crystal structure was further optimized by DFT-based computational methods. The positions of all heavy atoms from the crystal structure (including 8 oxygen atoms from water molecules, one Na^+ ion, and one K^+ ion) were fixed, and the structure was subjected to iterative optimization of the positions of the hydrogen atoms, with final optimization using the M06-2X method with the Def2TZVP basis set[106] in implicit water. The coordinates of the resultant hydrogen position-optimized structure are included in the Supporting Information.

In the full geometry optimization calculations using only implicit water, the structures were considered to have unrealistically close phosphate-amide hydrogen bonds (O•••H distances 1.67 Å), likely due to the limitations of implicit solvation in the solvation of anions. Therefore, the single-enantiomer crystal structure with hydrogen positions optimized and including water molecules was used as a starting point for full geometry optimization with explicit solvation. The molecules were truncated to convert the iodobenzoyl group into an acetyl group. In addition, the primary amide C-terminus ($–NH_2$) was converted into a dimethyl amide ($–NMe_2$) to avoid complications due to hydrogen bonding with the amide. In addition, for some optimizations the molecule was additionally truncated to convert the proline-NH_2 into a simple dimethyl amide, further simplifying the calculation. Full geometry optimization was conducted on the structures

Ac-pThr-NMe_2•$7H_2O$, Ac-pThr-Pro-NMe_2•$7H_2O$, and Ac-pThr-Pro-NH_2•$8H_2O$•K^+•Na^+. All calculations were conducted using pThr in the dianionic form. Final geometry optimization was conducted using the M06-2X functional and implicit water with the 6-311++G(3d,3p) basis set. All final calculations terminated normally. The resultant structures were broadly similar (similar final torsion angles) to those with fully implicit solvation, but had phosphate-amide hydrogen bond distances that were considered more realistic (O•••H distances 1.91–1.94 Å), and also that were more similar to those determined crystallographically with hydrogen position optimization.

Natural bond orbital (NBO) analysis[107] of the geometry-optimized Ac-pThr-NMe_2, Ac-pThr-Pro-NMe_2, Ac-pThr-NMe_2•$7H_2O$, Ac-pThr-Pro-NMe_2•$7H_2O$, and Ac-pThr-Pro-NH_2•$8H_2O$•K^+•Na^+structures at M06-2X level of theory with the 6-311+G(3d,3p) basis set in implicit water was conducted post-optimization to provide insights into the origins of the observed conformational preferences. The NBO method transforms a calculated wavefunction into localized form. The stabilization energies via eclipsing C–H/O–P bonds, $n\rightarrow\pi^*$, and phosphate-amide hydrogen bond interactions of the geometry-optimized structures were calculated by using NBO6[107] second-order perturbation theory as implemented Gaussian09. The relevant NBO orbitals were visualized using GaussView 5 with isovalues of 0.02.

Structures of the minimal molecules isopropyl phosphate and ethyl phosphate were analyzed via geometry optimization and via scans of the H–C–O–P torsion angle (equivalent to a scan of the χ_2 torsion angle in pThr or pSer, respectively), in order to understand the side-chain conformational preferences of pThr *versus* pSer. Geometry optimization was conducted at the MP2 level of theory with the 6-311++G(3d,3p) basis set in implicit water, in the dianionic, monoanionic, and neutral forms of the phosphate. Geometry-optimized structures were analyzed by frequency calculations, with no imaginary frequencies observed. These structures were then

subjected to H–C–O–P torsion angle scans, using the MP2 method and the 6-311++G(2d,2p) basis set in implicit water.

Supporting Information

Synthesis and characterization data for peptides, additional CD data, full 1–D ^{1}H NMR spectra, fingerprint regions of select TOCSY spectra, ^{1}H–^{13}C HSQC and ^{1}H–^{13}C HMBC spectra, ^{1}H-^{15}N HSQC spectra, ^{31}P NMR spectra, temperature-dependent NMR spectra, tabulations of NMR data, full results of the bioinformatics data, additional analysis of bioinformatics data, additional details and analysis of computational investigations, coordinates of calculated geometry-optimized structures, and additional details and coordinates of structures determined by X-ray crystallography. This information is available free of charge via the Internet at http://pubs.acs.org.

Addresses

[1] Department of Chemistry and Biochemistry, University of Delaware, Newark, DE 19716, United States

[2] Department of Chemistry, Indian Institute of Technology Ropar, Nangal Road 140001 India.

* To whom correspondence should be addressed. email: *zondlo@udel.edu*, phone: +1-302-831-0197; *sapatel@udel.edu*, phone: +1-302-831-6024; *gpyap@udel.edu,* phone: +1-302-831-4441.

‡ These authors contributed equally.

Acknowledgements

We thank NIH (GM93225, GM131302), NSF (MCB-1616490, CHE-2004110), and the DOD CDMRP PRARP program (AZ140115) for funding. We thank B. Kuhlman (UNC-Chapel Hill) for initial help with PDB analysis. We thank A. Brown, K. Thomas, and A. Bielska for preliminary CD experiments on JunD and Gsn1.

Figures

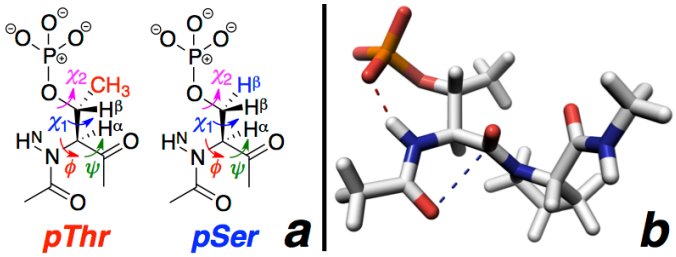

Figure 1. Phosphothreonine (pThr) and phosphoserine (pSer) residues. (a) Definitions of torsion angles and key nuclei analyzed in NMR experiments. Residues adjacent to pThr/pSer are omitted for clarity. (b) Structure of an Ac-pThr-Pro-NHMe dipeptide fragment from pdb 3a8x[2] (PKC-ι): pThr ϕ,ψ = –51°, +122°, χ_1 = –49° (*g*–), χ_2 = +112°. Hydrogen bond (red dashed line, 2.71 Å O•••N distance) and n→π* (blue dashed line, 2.83 Å O•••C distance) noncovalent interactions observed in this structure are indicated. This structure also has an eclipsed conformation at χ_2 (C–Hβ/O–P eclipsing, Hβ–C–O–P torsion angle –6°). Hydrogens were added in Pymol. The ylide structure of the dianionic phosphate (with a positive charge on P, negative charge on each O atom) is used here because it best represents the electronic structure of the phosphate, with each oxygen and phosphorous-oxygen bond equivalent in a structure with an approximately tetrahedral geometry. In subsequent Figures where data with both the monoanionic and dianionic forms of the phosphorylated amino acid are compared, the traditional (non-ylide) representation of the phosphate (with one P=O double bond) is employed due to the easier visual identification of the dianionic *versus* the monoanionic forms in that representation.

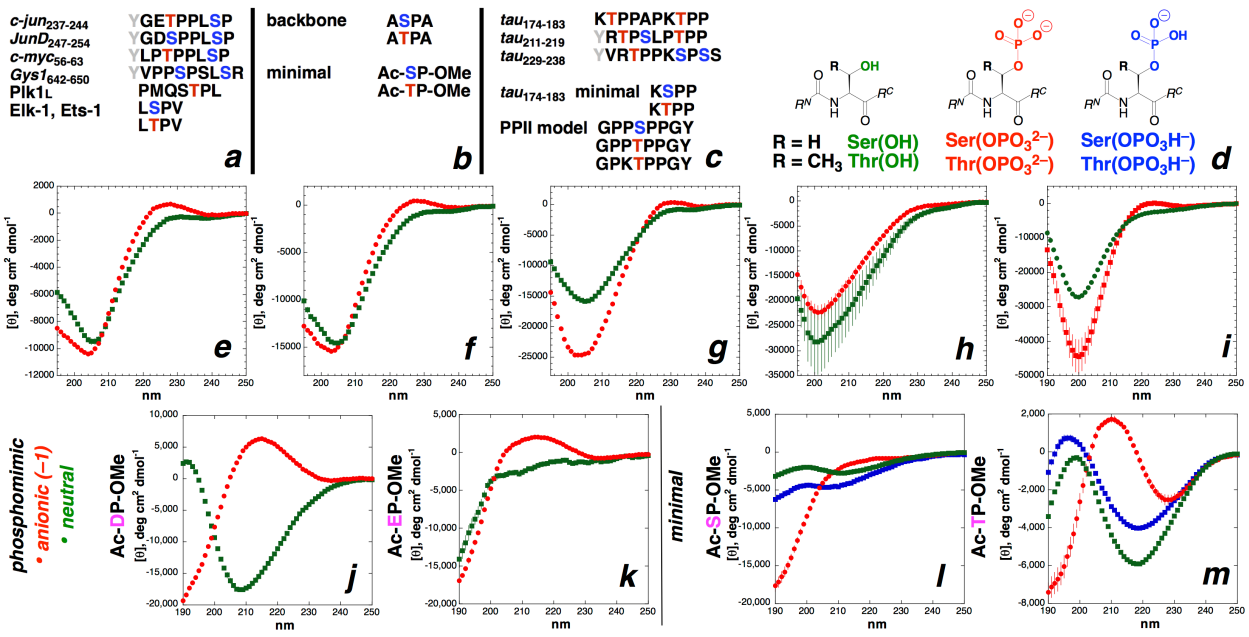

Figure 2. Peptide sequences and CD data. (a-c) Peptides examined. Phosphorylated Thr (blue) and Ser (red) residues are indicated. Tyr (grey) were added for concentration determination. All peptides were acetylated on the N-terminus and all peptides except dipeptides contained C-terminal amides. (a) Protein-derived peptides examined in this study. (b) Backbone and minimal peptides. (c) Tau-derived and proline-rich peptides examined previously.[25] The frequencies of these local sequences within the human proteome are substantial. The human proteome (uniprot.org, 20,996 protein sequences [July 20, 2018]) includes 15,893 proteins that contain an SP sequence (76% of all human proteins; 68,736 total SP sequences) and 13,927 proteins with a TP sequence (66% of all human proteins; 42,271 total TP sequences). 518 and 275 proteins have an ASPA or ATPA sequence; 723 and 441 proteins have a PSPP or PTPP sequence; 374 and 249 proteins have an LSPV or LTPV sequence; 186 and 189 proteins have a KSPP or KTPP sequence; and 205 and 186 proteins have an ESPP or ETPP sequence. (d) Structures of non-phosphorylated Ser and Thr, dianionic pSer ($pSer^{2-}$, pS^{2-}) and pThr ($pThr^{2-}$, pT^{2-}), and monoanionic pSer ($pSer^{-}$, pS^{-}) and pThr ($pThr^{-}$, pT^{-}). (e-i) CD spectra of non-phosphorylated

(green squares) and phosphorylated (red circles) peptides. An increase in the magnitude of the positive band around 220 nm indicates an increase in the population of PPII. (e) c-jun$_{237-244}$; (f) JunD$_{247-254}$; (g) c-myc$_{56-63}$; (h) glycogen synthase-1 Gys1$_{642-650}$; (i) optimized Plk1 polo-box domain ligand (Plk1$_L$). (j,k) CD spectra of minimal phosphomimetic peptides: neutral (green squares, pH 2) and anionic (red circles, pH 7) (j) Ac-DP-OMe and (m) Ac-EP-OMe. (l,m) CD spectra of minimal dipeptides: non-phosphorylated (green squares), monoanionic phosphorylated (blue squares, pH 4), and dianionic phosphorylated (red circles, pH 8) (l) Ac-Ser-Pro-OMe and (m) Ac-Thr-Pro-OMe. Experiments were conducted in phosphate-buffered saline at 2 ˚C (i) or 25 ˚C (all other peptides). See the Supporting Information for additional details, including additional CD spectra as a function of temperature and as a function of urea. CD spectra for peptides in Figure 2c are in refs. [24,25].

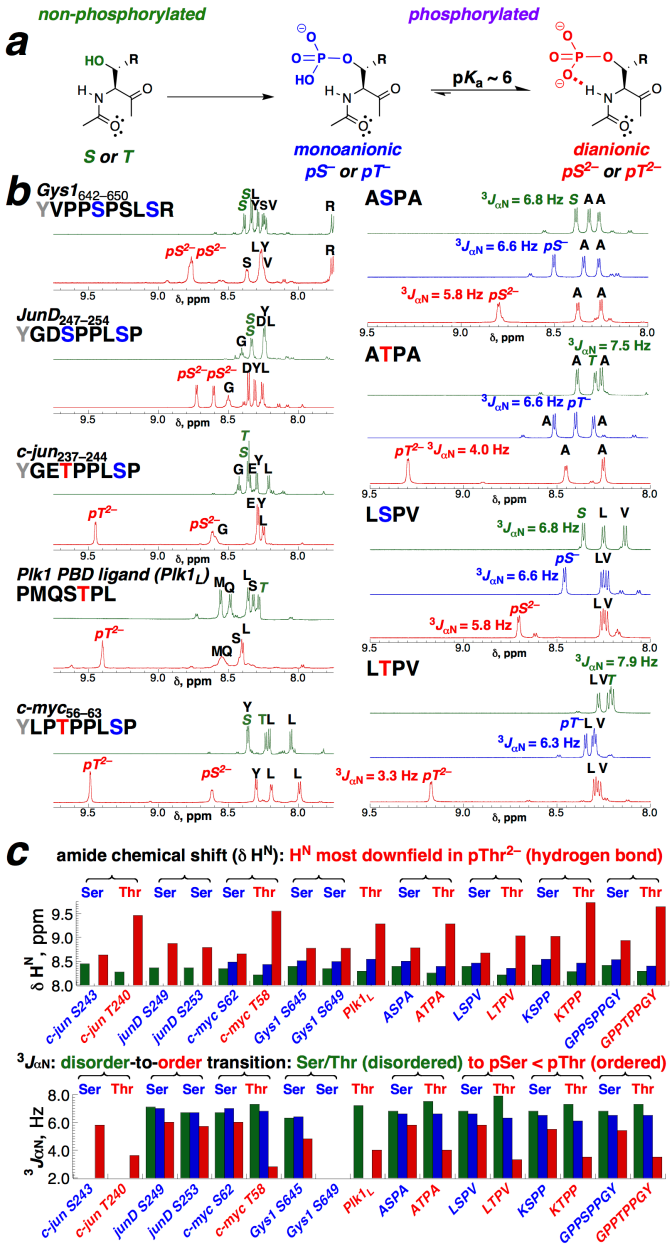

Figure 3. ^{1}H NMR data on peptides as a function of phosphorylation and ionization states. (a) Phosphorylation and ionization states of Ser and Thr, including the unmodified amino acid (green) and the monanionic (blue) and dianionic (red) ionization states of the phosphorylated amino acid. (b) 1-D NMR spectra of peptides. (c) Comparison of amide H chemical shifts (H^N δ) and H^N-Hα coupling constants ($^3J_{\alpha N}$) across all peptides. Primary NMR data for peptides from Figure 2c are in ref. [25]. Some $^3J_{\alpha N}$ values are missing due to spectral overlap. In protein-derived

peptides with more than one phosphorylation site (c-jun, junD, c-myc, Gys1), brackets indicate different phosphorylated amino acids in an individual peptide. In other peptides, brackets indicate comparisons between the Ser and Thr versions of those peptide contexts. All peptides contain small populations of *cis*-proline, which are observed as minor peaks in the NMR spectra. The analysis in Figure 3c is only on the major (all *trans*-proline) species. For all dipeptides and tetrapeptides with only one proline, $K_{trans/cis}$ was calculated; see the Supporting Information for details.

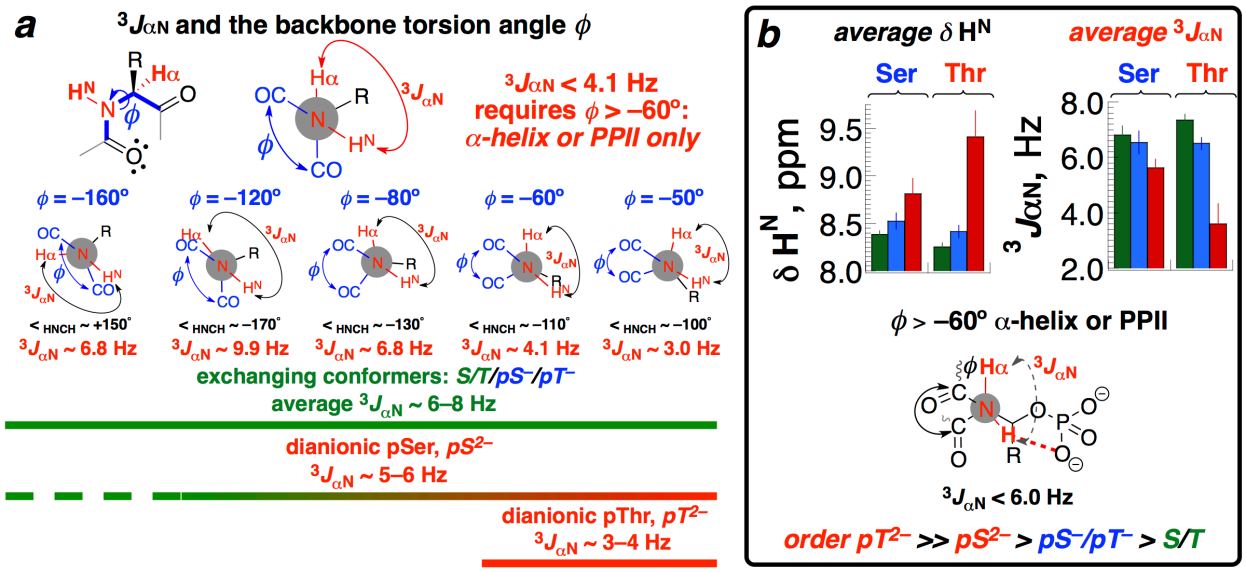

Figure 4. Analysis of $^{3}J_{\alpha N}$ NMR data at Ser/pSer and Thr/pThr residues across all peptides. (a) Correlation of the backbone torsion angle ϕ with the H^{N}–Hα 3-bond coupling constant $^{3}J_{\alpha N}$. Based on a parametrized Karplus relationship,[46] $^{3}J_{\alpha N}$ correlates with the ϕ torsion angle, with β-sheet exhibiting large $^{3}J_{\alpha N}$ (~8-10 Hz) and α-helix and PPII exhibiting smaller values of $^{3}J_{\alpha N}$. The maximum values of $^{3}J_{\alpha N}$ correspond with values of ϕ where the H^{N}–N–C–Hα torsion angle approaches 180° (ϕ ~ –130°; ϕ = torsion angle C(O)–N–Cα–C(O)) or 0° (ϕ ~ +50°), while the minimum values of $^{3}J_{\alpha N}$ correspond with values of ϕ where the H^{N}–N–C–Hα torsion angle approaches –90° (ϕ ~ –40°) or +90° (ϕ ~ +140°). However, due to conformational averaging, values between 4 and 10 Hz do not have unique solutions for $^{3}J_{\alpha N}$ on the left side of the Ramachandran plot. Broadly, given the preponderance of protein population on the left side of the Ramachandran plot, larger values of $^{3}J_{\alpha N}$ indicate more extended conformations in ϕ, while smaller values indicate more compact conformations in ϕ. Values between 6–8 Hz are consistent with random coil, due to population-weighted conformational averaging between the major backbone conformations (α, PPII, β). The further that $^{3}J_{\alpha N}$ is from these random coil values, the greater the overall order in the peptide. Values of $^{3}J_{\alpha N}$ < 4.1 Hz have unique solutions on the left side of the Ramachandran plot, indicating very compact values of ϕ and a high degree of order. (b) Average $^{3}J_{\alpha N}$ and H^{N} data across all peptides as a function of phosphorylation and ionization state.

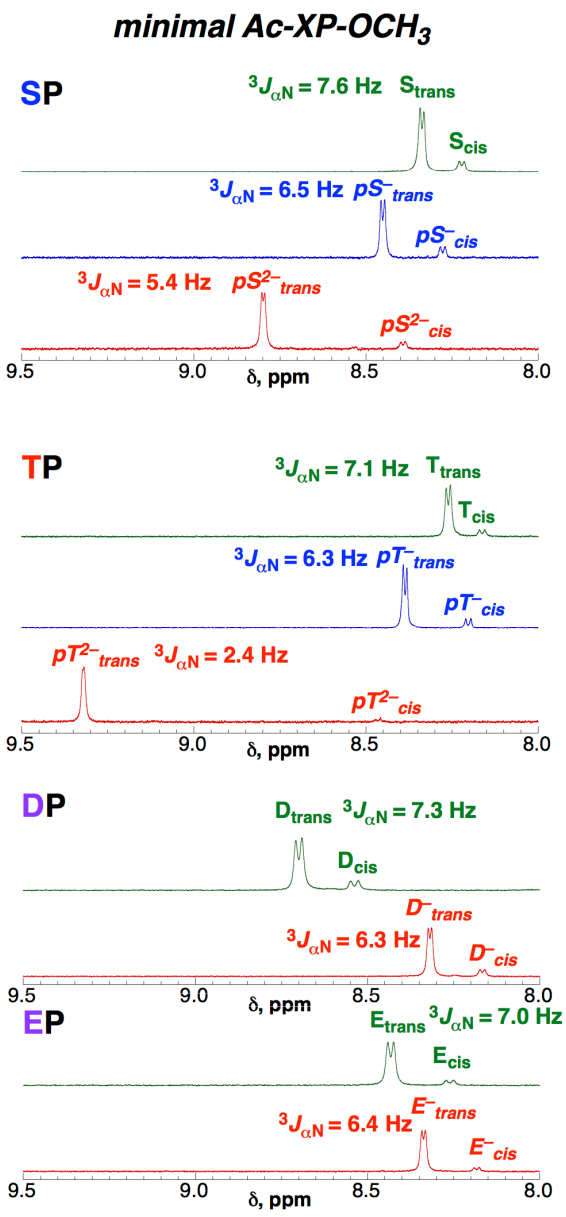

Figure 5. ^{1}H NMR data on minimal Ax-XP-OCH$_3$ dipeptides as a function of phosphorylation, ionization state, and/or phosphomimetic identity (pseudo-phosphorylation). Experiments were conducted on (top) the unmodified or neutral forms (green), the monoanionic forms (blue), and the dianionic forms (red) of Ser and Thr; and (bottom) the neutral (green) or anionic (red) forms of Asp and Glu. Further experimental details and tabulation of NMR data are in the Supporting Information.

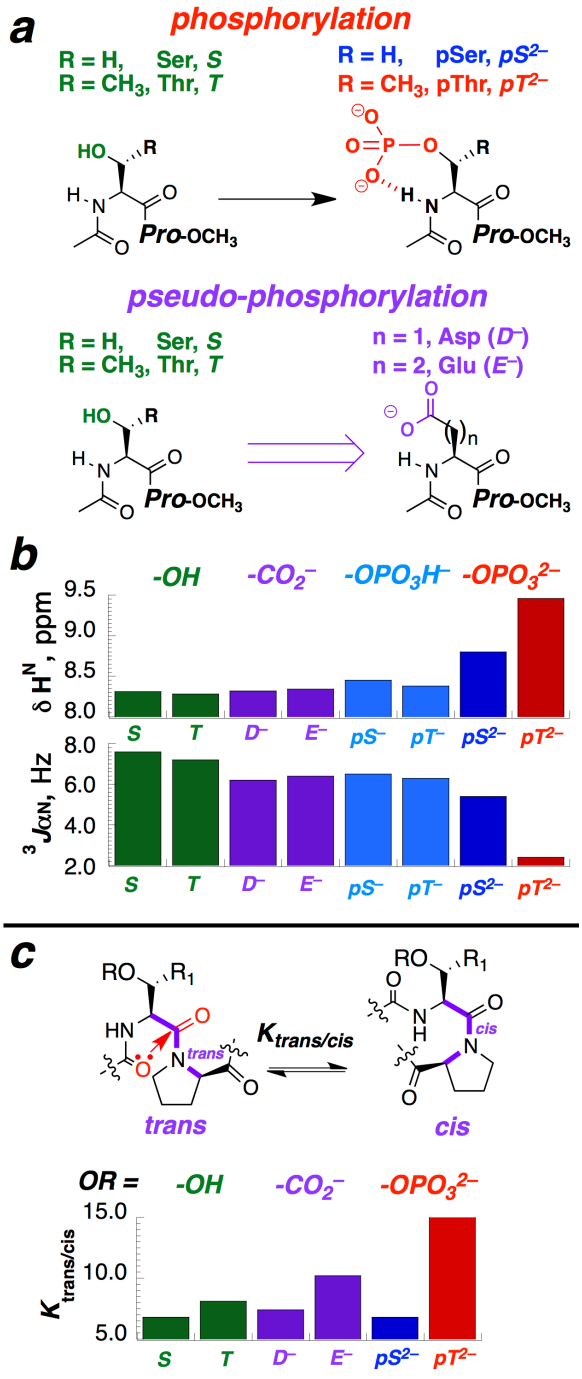

Figure 6. Summary of NMR data on minimal dipeptides Ac-X-Pro-OMe, as a function of residue identity, phosphorylation state, and ionization state. (a) Changes in structure of Ser and Thr when (top) phosphorylated or (bottom) replaced by the pseudophosphorylation mimics Asp and Glu. (b) Summary of the amide chemical shift (δ H^N) and $^3J_{\alpha N}$ values at the indicated residues in the indicated ionization states. (c) Summary of the ratio of *trans*-proline to *cis*-proline ($K_{trans/cis}$) in these dipeptides in the indicated ionization states.

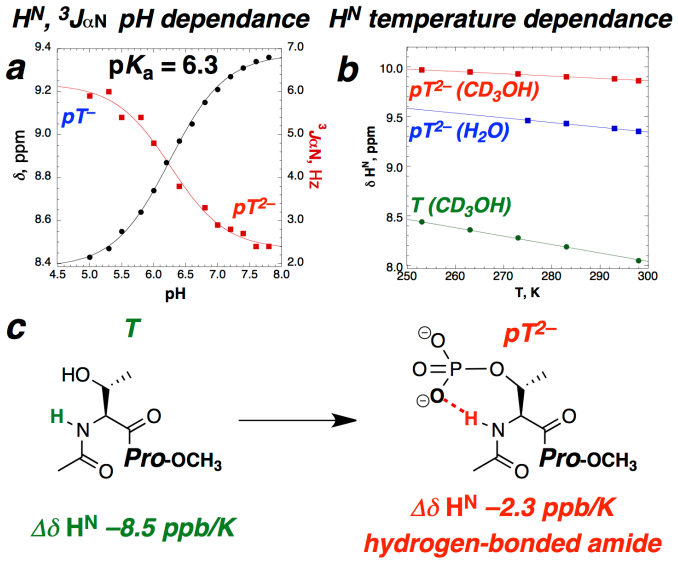

Figure 7. pH-dependent and temperature-dependent ^{1}H NMR data for Ac-Thr-Pro-OMe and Ac-pThr-Pro-OMe. (a) pH dependence of the pThr amide H (H^N) δ and the coupling constant between the pThr H^N and Hα ($^{3}J_{\alpha N}$). (b) Temperature dependence of H^N in H_2O and MeOH for Ac-Thr-Pro-OMe and Ac-pThr-Pro-OMe. MeOH was used to obtain a larger temperature range for the analysis, in order to obtain a more accurate value for the slope. (c) The data indicate a small temperature coefficient ($\Delta\delta > -5$ ppm, i.e. $|\Delta\delta| < 5$ ppm) for H^N of the peptide with pThr, consistent with the amide hydrogen being involved in a stable hydrogen bond.

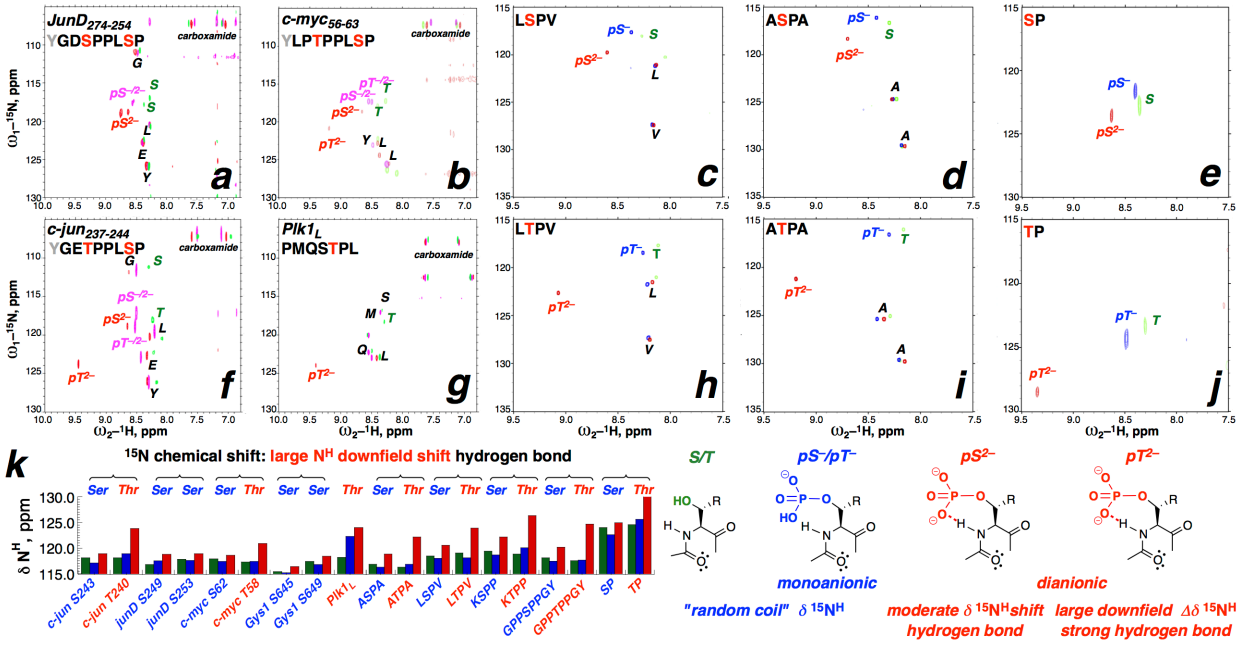

Figure 8. NMR data on peptides from 2-D heteronuclear NMR experiments. (a-j) ^{1}H-^{15}N HSQC spectra and data correlating amide hydrogen (H^N) and amide nitrogen (N^H) chemical shifts, for (a) JunD, (b) c-myc, (c) LSPV, (d) ASPA, (e) SP, (f) c-jun, (g) $Plk1_L$, (h) LPTV, (i) ATPA, and (j) TP peptides, as a function of phosphorylation state and ionization state. In each case, green indicates the peptide with unmodified Ser or Thr, blue indicates the peptide with pSer and/or pThr in the monoanionic form (pH 4), magenta indicates the peptide with pSer and/or pThr in a mixed ionic state (both –1 and –2 states present, corresponding with data at pH 6 or pH 6.5; see the Supporting Information for details); and blue indicates the peptide with pSer or pThr predominantly in the dianionic state (pH 7.2). Additional experimental details and larger spectra with tabulated chemical shifts are in the Supporting Information. Primary and tabulated data for a subset of peptides from Figure 2c are in ref. [25]. (k) Summary of Ser and Thr ^{15}N chemical shift data across the peptides, as a function of phosphorylation state and phosphate ionization state.

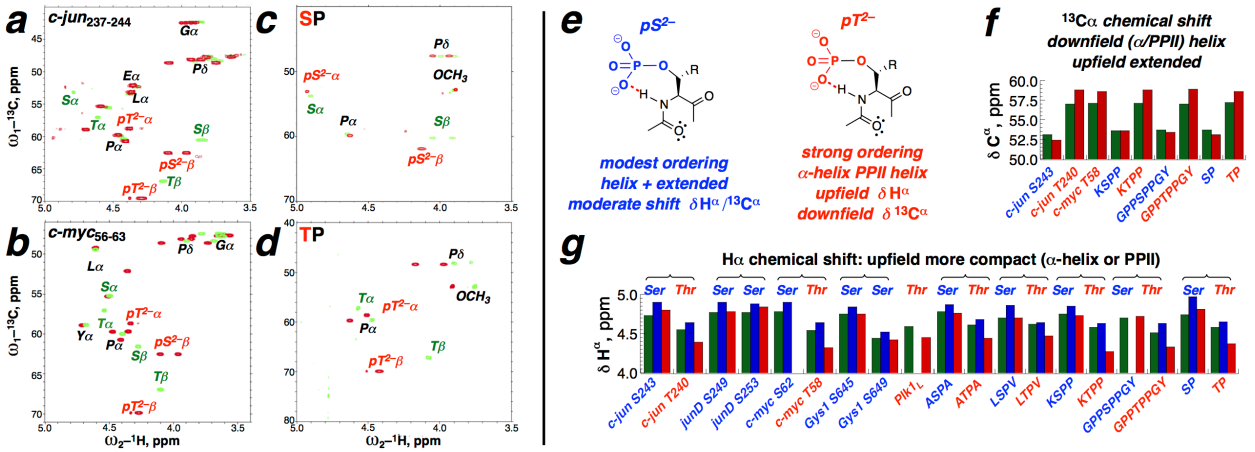

Figure 9. NMR data on peptides from ^{1}H-^{13}C HSQC spectra to correlate Hα and Cα chemical shifts. (a-d) H-^{13}C HSQC spectra from selected peptides, comparing the non-phosphorylated (green) and phosphorylated (red) peptides. (e) Summary and interpretation of chemical shift changes in pSer versus pThr. (f) Summary of ^{13}Cα chemical shift data for non-phosphorylated (green) and phosphorylated (red) peptides. (g) Summary of ^{1}Hα chemical shift data for non-phosphorylated (green), monoanionic phosphorylated (blue), and dianionic phosphorylated (red) peptides. Tabulated data from individual spectra, larger versions of the spectra, and experimental details are in the Supporting Information. Primary and tabulated data for a subset of peptides from Figure 2c are in ref. [25].

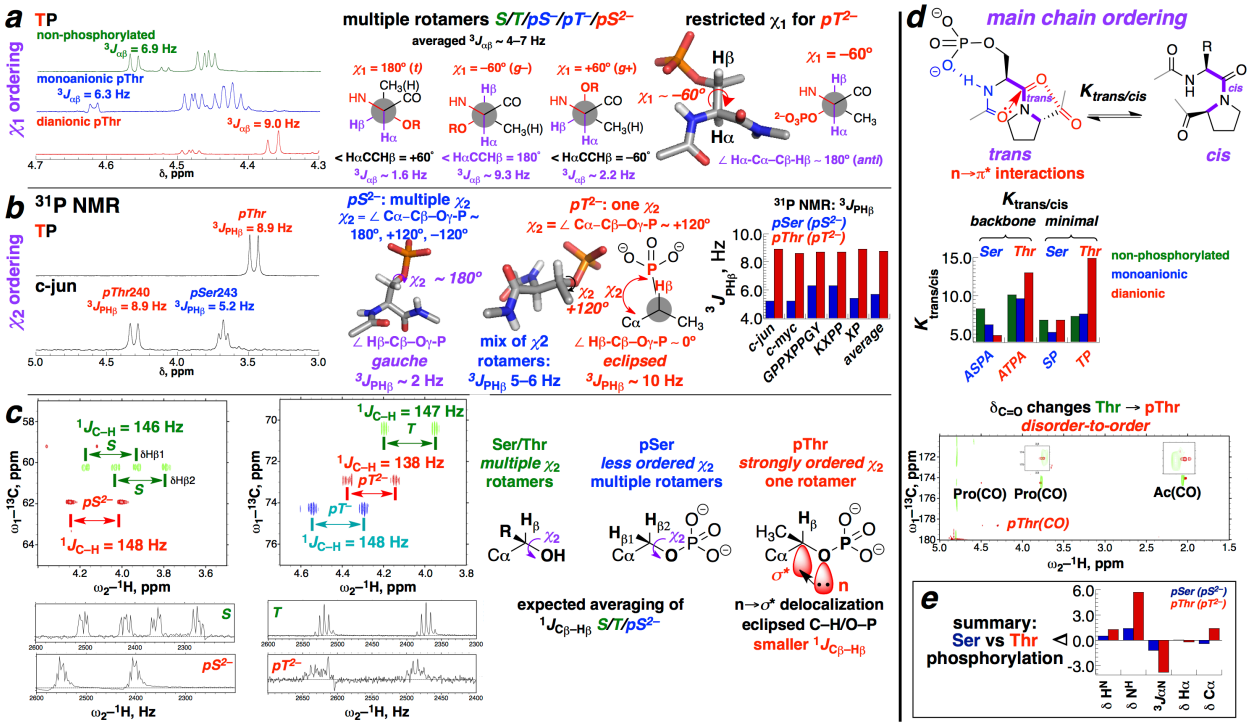

Figure 10. NMR data to identify the effects of phosphorylation on torsion angles of the side chain (χ_1 and χ_2) and main chain (ω). (a) ^{1}H NMR spectra (Hα region) of Ac-pThr-Pro-OMe at pH 8 in 100% D_2O, with $^3J_{\alpha\beta}$ indicated. In D_2O, the D on the amide N (N–D bond) allows the direct measurement of $^3J_{\alpha\beta}$ as a simple coupling constant, without complications from further coupling with the amide H^N. (b) ^{31}P NMR spectra in 100% D_2O, with $^3J_{PH\beta}$ quantified. (c) Effects of phosphorylation on $^1J_{H\beta C\beta}$. (d) Effects of phosphorylation in model peptides on *trans* versus *cis* proline amide bond ($K_{trans/cis}$; ω torsion angle) and on carbonyl ^{13}C δ, the latter determined via ^{1}H-^{13}C HMBC experiments. (e) Summary of NMR data across all peptides in Figure 2abc as a function of amino acid (Ser vs Thr) and phosphorylation and ionization states. Primary and tabulated data for a subset of peptides from Figure 2c are in the Supporting Information of ref. [25]. Analysis of $^3J_{\alpha\beta}$ and $^3J_{PH\beta}$ on pThr in α-helical peptides as a function of helix position was also conducted in ref. [26], where similar results were observed for pThr.

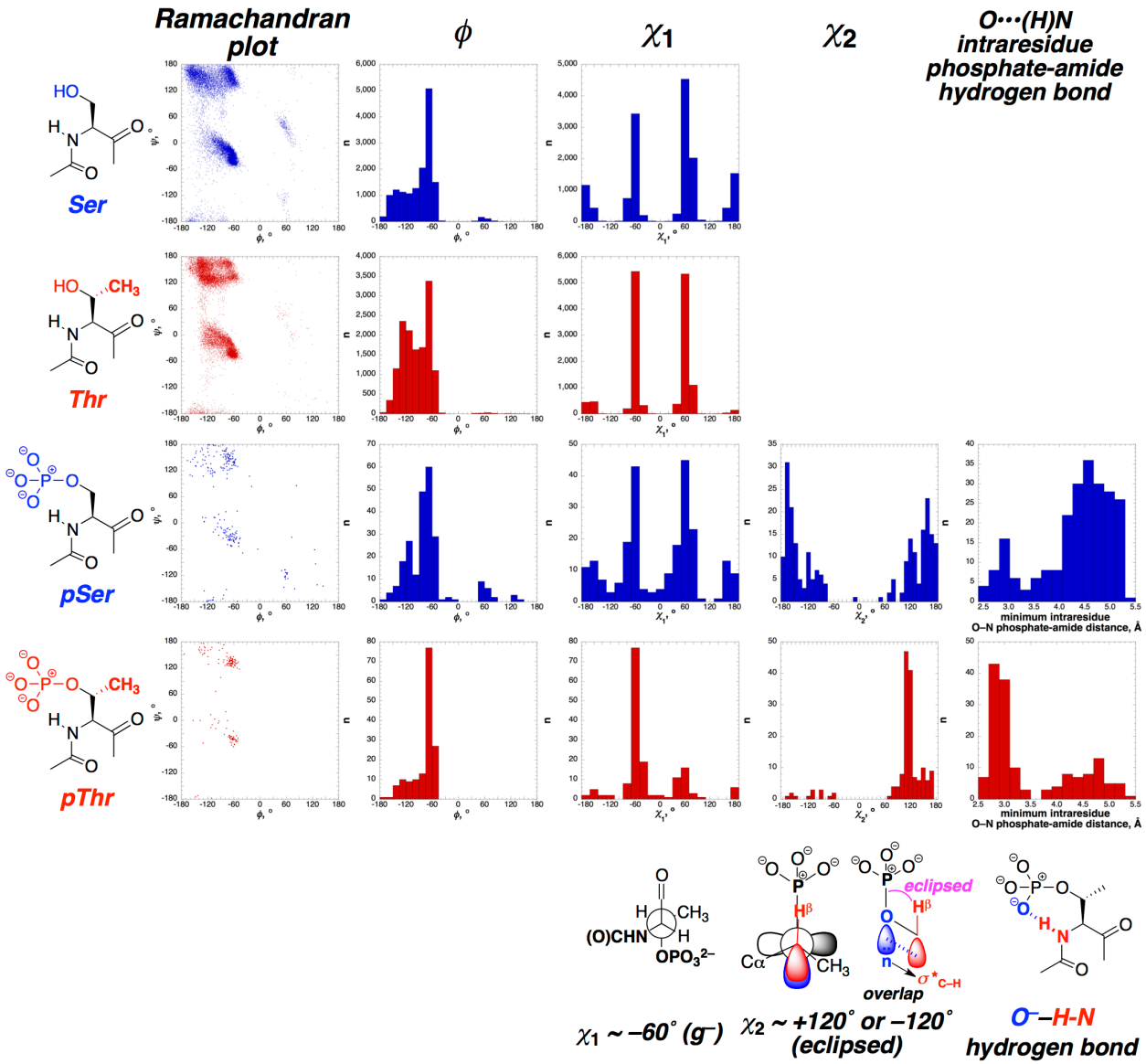

Figure 11. Analysis of Ser (top, blue), Thr (top, red), pSer (bottom, blue), and pThr (bottom, red) residues in the PDB. From left to right: amino acid structure; Ramachandran plot; histograms of ϕ, χ_1, and χ_2 torsion angles; and histogram of shortest distance between any phosphate oxygen and the amide nitrogen of the same residue (intraresidue hydrogen bond distance between heavy atoms for structures with O•••N distances < 3.5 Å). Tabulation of all bioinformatics data on phosphopeptides is in Table S1 and Table S2.

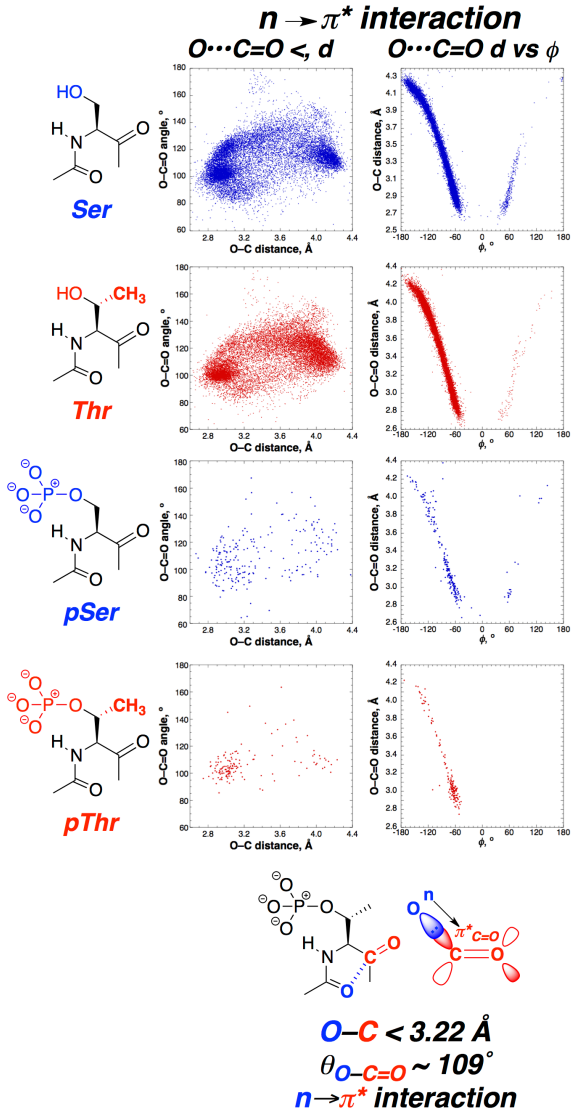

Figure 12. Analysis of n→π* interaction parameters for Ser (top, blue), Thr (top, red), pSer (bottom, blue), and pThr (bottom, red) residues in the PDB. (left) Plots of O_i•••C_{i+1}=O angle versus O_i•••C_{i+1} distance between consecutive carbonyls. (right) Plots of O_i•••C_{i+1} intercarbonyl n→π* distance versus the ϕ main chain torsion angle. An n→π* interaction is defined by an O_i•••C_{i+1} distance < 3.22 Å and an O_i•••C_{i+1}=O angle θ with 99° ≤ θ ≤ 119°, with shorter distances and θ closer to 109° indicating a more favorable n→π* interaction.

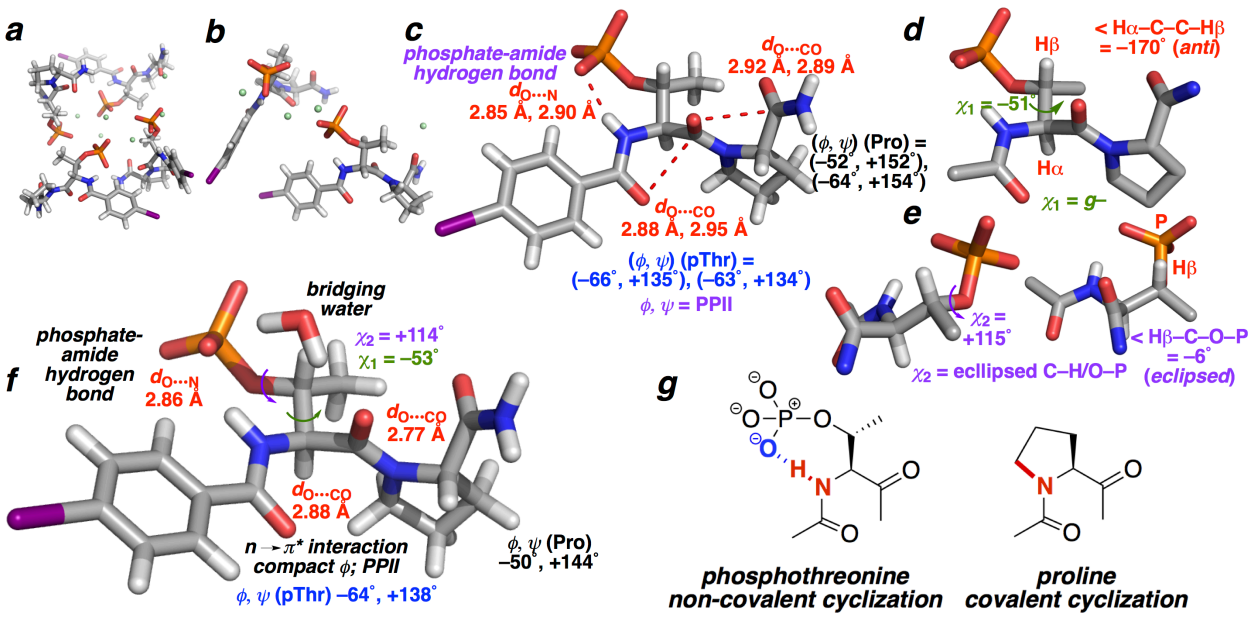

Figure 13. Structures of dianionic (a-e) (±)-4-I-Bz-pThr-Pro-NH_2 (resolution 0.87 Å) and (f) single-enantiomer 4-I-Bz-pThr-Pro-NH_2 (resolution 0.80 Å), as determined by X-ray crystallography. (a) Crystal packing showing 4 molecules, two L-peptides and two D-peptides (the asymmetric unit plus its mirror image). Water molecules (10 per asymmetric unit) found in the crystal structure are omitted for clarity. Sodium atoms are indicated in green. (b) Asymmetric unit (P_{-1} centrosymmetric space group), containing one molecule of L-peptide and one of D-peptide, with distinct (not symmetrically related) structures. (c) Structure of one molecule of 4-I-Bz-pThr-Pro-NH_2, with torsion angles and distances from both structures indicated. (d,e) Analysis of (d) χ_1 and (e) χ_2 torsion angles in one molecule of the structure. The torsion angles of the D-peptide were inverted to those of its L-peptide equivalent for clarity. (f) Single-enantiomer crystal structure of 4-I-Bz-pThr-Pro-NH_2. Additional water molecules and sodium and potassium ions are omitted for clarity. In addition, the structures indicate significant puckering at the pThr and Pro carbonyls, but not at the iodobenzoyl carbonyl, consistent with the participation of the acceptor carbonyls in an n→π* interaction. The bridging water molecule observed in (f) exhibits close (2.9 Å O•••O distances) hydrogen bonds with both one phosphate oxygen and the pThr carbonyl. To our knowledge, this bridging water molecule has not previously been observed. In addition, a version of the single-enantiomer structure has been generated using DFT calculations to optimize the positions of the hydrogens (while fixing the positions of the heavy atoms based on those determined crystallographically), which provides better accuracy of hydrogen atom

positions than is determined directly by X-ray crystallography.[73] In this hydrogen geometry-optimized structure (M06-2X/Def2TZVP/H_2O), which includes 8 H_2O molecules, one K^+ atom, and one Na^+ atom, the pThr amide N–H bond length is 1.018 Å, with a phosphate-amide O•••HN hydrogen bond distance of 1.88 Å. The Hβ–Cβ–O–P torsion angle is 4.5° (χ_2 = 113.8°), essentially a fully eclipsed conformation. The phosphateO•••HOH and HOH•••O=C distances in the bridging water molecule are 1.95 Å and 1.91 Å, respectively. See the Supporting Information and Table 2 for details. (g) Comparison of the non-covalently cyclic preferred structure of dianionic pThr and the covalently cyclic structure of Pro. While the ring sizes of Pro (5) and pThr (7) are different, the effects of non-covalent cyclization in dianionic pThr are to restrict the available conformations and to render its amide H unavailable for hydrogen bonding to other groups within the protein, functionally similar to the absence of an amide H in proline. We previously observed[26] that phosphorylation of Thr to pThr at a central position of an α-helical peptide completely eliminates α-helicity in the peptide, to an extent similar to that of changing Thr to Pro in an α-helix.

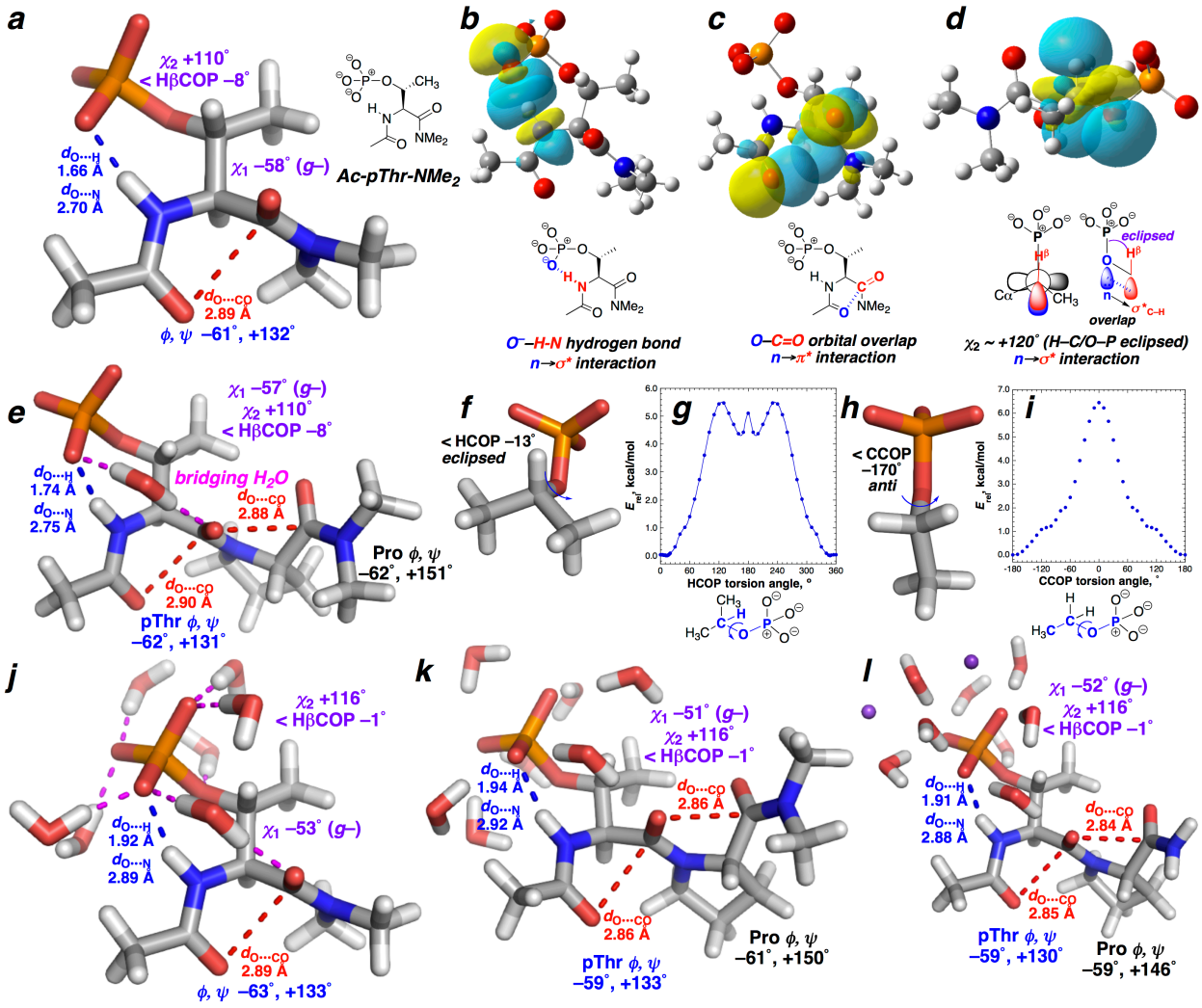

Figure 14. Computational investigation of the structure and interactions stabilizing phosphothreonine. (a) Structure resulting from geometry optimization of Ac-pThr-NMe_2. All peptide models were generated using the M06-2X method and the 6-311++G(3d,3p) basis set in implicit H_2O. (b-d) Natural bond orbital (NBO) analysis of Ac-pThr-NMe_2, indicating the molecular orbital basis of stabilizing non-covalent interactions in pThr. Stabilization is provided by electron delocalization that occurs via overlap of orbital lobes. Favorable electrostatics also contribute to stabilization. Via NBO analysis, the n→π* interaction is stabilized by 0.8 kcal mol^{-1} [1] via electron delocalization between the acyl carbonyl p-like lone pair and the pThr carbonyl π*

molecular orbitals, while the n→σ* interaction that stabilizes the eclipsed conformation is favorable by 4.6 kcal mol^{-1}. NBO analysis also indicates stabilization of the eclipsed χ_2 conformation via σ→σ* electron delocalization between the O–P σ and the C–Hβ σ* (1.6 kcal mol^{-1}). (e) Structure of Ac-pThr-Pro-NMe_2•H_2O. (f-i) Geometry-optimized structures (f, h) and torsion angle scans equivalent to χ_2 (g,i) on dianionic (f, g) isopropyl phosphate (pThr model) and (h, i) ethyl phosphate (pSer model). Geometry optimization was conducted using the MP2 method and (f,h) 6-311++G(3d,3p) or (g,i) 6-311++G(2d,2p) basis sets in implicit H_2O. (j,k.l) Geometry optimization of the truncated forms of the single-enantiomer crystal structure, including the explicit solvation observed crystallographically, with (j) Ac-pThr-NMe_2•$7H_2O$, (k) Ac-pThr-Pro-NMe_2•$7H_2O$, and (l) Ac-pThr-Pro-NH_2•$8H_2O$•K^+•Na^+. These structures with explicit solvation had torsion angles similar to those determined using fully implicit solvation. However, the respective phosphate-amide hydrogen bond distances were deemed significantly more reasonable in the structures with explicit solvation. In addition, the χ_2 torsion angle was essentially fully eclipsed (∠ Hβ–C–O–P = –1°) in these structures with explicit solvation.

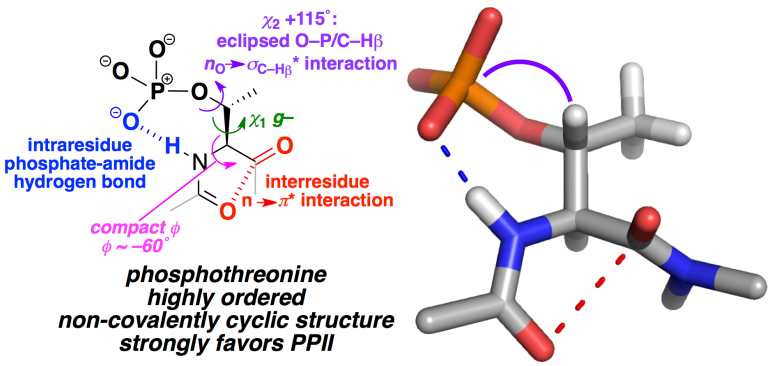

Figure 15. Summary of the key structural features of the predominant conformation of dianionic phosphothreonine. The overall structure is bicyclic via noncovalent interactions (phosphate-amide hydrogen bond and n→π* interaction).

Tables

Table 1. Average values of NMR-derived data at 25 ˚C for all peptides in Figure 2a-c. Data for monoanionic phosphorylated peptides were collected at pH 4. Data for dianionic phosphorylated peptides were collected at pH 7.5-8.0. Changes (Δ) indicate the change in the indicated value from the non-phosphorylated residue to the dianionic phosphorylated residue.

	S Ser(OH)	*pS*$^{-}$ Ser(OPO_3H^-)	*pS*$^{2-}$ Ser(OPO_3^{2-})	*T* Thr(OH)	*pT*$^{-}$ Thr(OPO_3H^-)	*pT*$^{2-}$ Thr(OPO_3^{2-})	**Δ, S to pS^{2-}**	**Δ, T to pT^{2-}**
H^N δ, ppm	8.37	8.52	8.87	8.25	8.44	9.51	**+0.50**	**+1.26**
N^H δ, ppm	118.2	117.4	119.5	118.3	119.4	124.0	**+1.3**	**+5.7**
$^3J\alpha_N$, Hz	6.8	6.4	5.6	7.3	6.5	3.5	**–1.2**	**–3.8**
Hα δ, ppm	4.65	4.82	4.68	4.55	4.60	4.34	**+0.03**	**–0.21**
Cα δ, ppm	53.4	n.d.	53.0	57.1	n.d.	58.5	**–0.4**	**+1.4**

Table 2. Comparison of key structural features of pThr and pSer as determined by geometry optimization calculations (top) and as observed by X-ray crystallography (bottom).

	pThr/pSer								*Pro*			C=O pyramid.		
			d, Å n→π*	*d*, Å H bond				<			*d*, Å n→π*	torsion <, Cα-N-O-C		
peptide	***ϕ*, °**	***ψ*, °**	**O···C**	**O···HN**	**H–N**	**χ_1, °**	**χ_2, °**	**HCOP**	***ϕ*, °**	***ψ*, °**	**O···C**	**Ac, °**	**pX, °**	**Pro, °**
Ac-pThr-NMe_2	-61	132	2.89	1.67	1.04	-58	110	-8	–	–	–	0.3	3.0	–
Ac-pThr-NMe_2•H_2O	-59	133	2.87	1.73	1.03	-52	111	-7	–	–	–	0.3	2.4	–
Ac-pThr-Pro-NMe_2	-63	129	2.92	1.67	1.04	-58	110	-7	-62	149	2.86	0.3	2.2	2.1
Ac-pThr-Pro-NMe_2•H_2O	-62	131	2.90	1.74	1.03	-52	112	-6	-62	151	2.88	0.1	2.2	2.4
Ac-pThr-NMe_2•$7H_2O$	-63	133	2.89	1.92	1.02	-53	116	-1	–	–	–	0.4	2.1	–
Ac-pThr-Pro-NMe_2•$7H_2O$	-59	133	2.86	1.94	1.02	-51	116	-1	-61	150	2.86	0.6	2.6	2.0
Ac-pThr-Pro-NH_2•$8H_2O$•Na^+•K^+	-59	130	2.85	1.91	1.02	-52	116	-1	-59	146	2.84	0.3	2.6	2.7
Ac-pSer-NMe_2	-64	151	2.95	1.68	1.04	-59	109	-12	–	–	–	0.4	2.5	–
Ac-pSer-NMe_2 χ_1 χ_2 *t*	-65	140	3.00	–	1.01	-178	-174	-55	–	–	–	-0.3	0.8	–
Ac-pSer-NMe_2•H_2O	-63	148	2.93	1.74	1.03	-54	111	-10	–	–	–	0.3	2.4	–
Ac-pSer-Pro-NMe_2	-67	151	2.99	1.69	1.04	-59	109	-12	-59	150	2.84	0.4	2.7	2.1
XRC														
4-I-Bz-pThr-Pro-NH_2•H_2O	-64	138	2.88	1.91*	1.015*	-53	114	-5	-50	144	2.77	0.5	1.4	2.2
4-I-Bz-pThr-Pro-NH_2	-67	135	2.95	1.94*	1.015*	-51	115	-6	-52	152	2.89	-0.3	1.6	1.8
4-I-Bz-pThr-Pro-NH_2	-63	134	2.88	1.88*	1.015*	-51	115	-5	-64	154	2.92	0.6	2.6	2.1
4-I-Bz-pThr-Pro-NH_2•H_2O[a]	-64	138	2.88	1.88	1.018	-53	114	-4	-50	144	2.77	0.5	1.4	2.2

[a] Single-enantiomer crystal structure with hydrogen positions optimized by DFT (M06-2X functional, Def2TZVP basis set, implicit H_2O). All full geometry optimization calculations were conducted using the M06-2X functional and the 6-311++G(3d,3p) basis set in implicit H_2O. Structures with •H_2O appended to the peptide sequence include one bridging H_2O molecule, as observed in the single-enantiomer crystal structure. All torsion angles in the D-peptide in the racemic crystal structure were converted to their mirror image (L-peptide) values for clearer comparison. * Distances were determined via normalization of the lengths of bonds to hydrogen.

References

(1) Manning, G.; Whyte, D. B.; Martinez, R.; Hunter, T.; Sudarsanam, S. The protein kinase complement of the human genome. *Science* **2002**, *298*, 1912-1934.

(2) Takimura, T.; Kamata, K.; Fukasawa, K.; Oshawa, H.; Komatani, H.; Yoshizumi, T.; Takahashi, I.; Kotani, H.; Iwasawa, Y. Structures of the PKC-iota Kinase Domain in Its ATP-Bound and Apo Forms Reveal Defined Structures of Residues 533-551 in the C-terminal Tail and their Roles in Binding. *Acta Crystallogr., Sect. D.* **2010**, *66*, 577-.

(3) Ubersax, J. A.; Ferrell, J. E. Mechanisms of specificity in protein phosphorylation. *Nat. Rev. Mol. Cell. Biol.* **2007**, *8*, 530-541.

(4) Shaw, R. J.; Lamia, K. A.; Vasquez, D.; Koo, S. H.; Bardeesy, N.; DePinho, R. A.; Montminy, M.; Cantley, L. C. The kinase LKB1 mediates glucose homeostasis in liver and therapeutic effects of metformin. *Science* **2005**, *310*, 1642-1646.

(5) Durocher, D.; Taylor, I. A.; Sarbassova, D.; Haire, L. F.; Westcott, S. L.; Jackson, S. P.; Smerdon, S. J.; Yaffe, M. B. The molecular basis of FHA Domain : Phosphopeptide binding specificity and implications for phospho-dependent signaling mechanisms. *Mol. Cell* **2000**, *6*, 1169-1182.

(6) Pennell, S.; Westcott, S.; Ortiz-Lombardia, M.; Patel, D.; Li, J. J.; Nott, T. J.; Mohammed, D.; Buxton, R. S.; Yaffe, M. B.; Verma, C.; Smerdon, S. J. Structural and Functional Analysis of Phosphothreonine-Dependent FHA Domain Interactions. *Structure* **2010**, *18*, 1587-1595.

(7) Gao, X. L.; Wang, H. Z.; Yang, J. J.; Liu, X. W.; Liu, Z. R. Pyruvate Kinase M2 Regulates Gene Transcription by Acting as a Protein Kinase. *Mol. Cell* **2012**, *45*, 598-609.

(8) Keller, K. E.; Tan, I. S.; Lee, Y. S. SAICAR Stimulates Pyruvate Kinase Isoform M2 and Promotes Cancer Cell Survival in Glucose-Limited Conditions. *Science* **2012**, *338*, 1069-1072.

(9) Yang, W. W.; Xia, Y.; Hawke, D.; Li, X. J.; Liang, J.; Xing, D. M.; Aldape, K.; Hunter, T.; Yung, W. K. A.; Lu, Z. M. PKM2 Phosphorylates Histone H3 and Promotes Gene Transcription and Tumorigenesis. *Cell* **2012**, *150*, 685-696.

(10) Keller, K. E.; Doctor, Z. M.; Dwyer, Z. W.; Lee, Y. S. SAICAR Induces Protein Kinase Activity of PKM2 that Is Necessary for Sustained Proliferative Signaling of Cancer Cells. *Mol. Cell* **2014**, *53*, 700-709.

(11) Chen, C.; Ha, B. H.; Thévenin, A. F.; Lou, H. J.; Zhang, R.; Yip, K. Y.; Peterson, J. R.; Gerstein, M.; Kim, P. M.; Filippakopoulos, P.; Knapp, S.; Boggon, T. J.; Turk, B. E. Identification of a Major Determinant for Serine-Threonine Kinase Phosphoacceptor Specificity. *Mol. Cell* **2014**, *53*, 140-147.

(12) Chen, S.; Chen, F.; Li, W. Phosphorylated and non-phosphorylated serine and threonine residues evolve at different rates in mammals. *Mol. Biol. Evol.* **2010**, *27*, 2548-2554.

(13) Yaffe, M. B.; Rittinger, K.; Volinia, S.; Caron, P. R.; Aitken, A.; Leffers, H.; Gamblin, S. J.; Smerdon, S. J.; Cantley, L. C. The structural basis for 14-3-3 : phosphopeptide binding specificity. *Cell* **1997**, *91*, 961-971.

(14) Verdecia, M. A.; Bowman, M. E.; Lu, K. P.; Hunter, T.; Noel, J. P. Structural basis for phosphoserine-proline recognition by group IV WW domains. *Nature Struct. Biol.* **2000**, *7*, 639-643.

(15) Yaffe, M. B.; Eila, A. E. H. Phosphoserine/threonine-binding domains. *Curr. Opin. Cell. Biol.* **2001**, *13*, 131-138.

(16) Manke, I. A.; Lowery, D. M.; Nguyen, A.; Yaffe, M. B. BRCT repeats as phosphopeptide-binding modules involved in protein targeting. *Science* **2003**, *302*, 636-639.

(17) Tholey, A.; Lindemann, A.; Kinzel, V.; Reed, J. Direct effects of phosphorylation on the preferred backbone conformation of peptides: A nuclear magnetic resonance study. *Biophysical J.* **1999**, *76*, 76-87.

(18) Bienkiewicz, E. A.; Lumb, K. J. Random-coil chemical shifts of phosphorylated amino acids. *J. Biomol. NMR* **1999**, *15*, 203-206.

(19) Du, J.-T.; Li, Y.-M.; Wei, W.; Wu, G.-S.; Zhao, Y.-F.; Kanazawa, K.; Nemoto, T.; Nakanishi, H. Low-barrier hydrogen bond between phosphate and the amide group in phosphopeptide. *J. Am. Chem. Soc.* **2005**, *127*, 16350-16351.

(20) Lee, K. K.; Kitn, E.; Joo, C.; Song, J.; Han, H.; Cho, M. Site-selective Intramolecular Hydrogen-Bonding Interactions in Phosphorylated Serine and Threonine Dipeptides. *J. Phys. Chem. B* **2008**, *112*, 16782-16787.

(21) Narayanan, A.; Jacobson, M. P. Computational studies of protein regulation by post-translational phosphorylation. *Curr. Opin. Struct. Biol.* **2009**, *19*, 156-163.

(22) Hendus-Altenburger, R.; Fernandes, C. B.; Bugge, K.; Kunze, M. B. A.; Boomsma, W.; Kragelund, B. B. Random coil chemical shifts for serine, threonine and tyrosine phosphorylation over a broad pH range. *J. Biomol. NMR* **2019**, *73*, 713-725.

(23) Mateos, B.; Holzinger, J.; Conrad-Billroth, C.; Platzer, G.; Zerko, S.; Sealey-Cardona, M.; Anrather, D.; Kozminski, W.; Konrat, R. Hyperphosphorylation of Human Osteopontin and Its Impact on Structural Dynamics and Molecular Recognition. *Biochemistry* **2021**, *60*, 1347-1355.

(24) Bielska, A. A.; Zondlo, N. J. Hyperphosphorylation of tau induces local polyproline II helix. *Biochemistry* **2006**, *45*, 5527-5537.

(25) Brister, M. A.; Pandey, A. K.; Bielska, A. A.; Zondlo, N. J. OGlcNAcylation and Phosphorylation Have Opposing Structural Effects in tau: Phosphothreonine Induces Particular Conformational Order. *J. Am. Chem. Soc.* **2014**, *136*, 3803-3816.

(26) Elbaum, M. B.; Zondlo, N. J. OGlcNAcylation and Phosphorylation Have Similar Structural Effects in α-Helices: Post-Translational Modifications as Inducible Start and Stop Signals in α-Helices, with Greater Structural Effects on Threonine Modification. *Biochemistry* **2014**, *53*, 2242-2260.

(27) Lovell, S. C.; Word, J. M.; Richardson, J. S.; Richardson, D. C. The Penultimate Rotamer Library. *Proteins* **2000**, *40*, 389-408.

(28) Andrew, C. D.; Warwicker, J.; Jones, G. R.; Doig, A. J. Effect of phosphorylation on a-helix stability as a function of position. *Biochemistry* **2002**, *41*, 1897-1905.

(29) Signarvic, R. S.; DeGrado, W. F. De Novo Design of a Molecular Switch: Phosphorylation-Dependent Association of Designed Peptides. *J. Mol. Biol.* **2003**, *334*, 1-12.

(30) Rani, L.; Mallajosyula, S. S. Site-Specific Stabilization and Destabilization of alpha Helical Peptides upon Phosphorylation and O-GlcNAcylation. *J. Phys. Chem. B* **2021**, *125*, 13444-13459.

(31) Szilak, L.; Moitra, J.; Krylov, D.; Vinson, C. Phosphorylation destabilizes a-helices. *Nature Struct. Biol.* **1997**, *4*, 112-114.

(32) Szilak, L.; Moitra, J.; Vinson, C. Design of a leucine zipper coiled coil stabilized 1.4 kcal mol^{-1} by phosphorylation of a serine in the e position. *Protein Sci.* **1997**, *6*, 1273-1283.

(33) Smith, C. K.; Withka, J. M.; Regan, L. A Thermodynamic Scale for the Beta-Sheet Forming Tendencies of the Amino-Acids. *Biochemistry* **1994**, *33*, 5510-5517.

(34) Minor, D. L.; Kim, P. S. Measurement of the Beta-Sheet-Forming Propensities of Amino-Acids. *Nature* **1994**, *367*, 660-663.

(35) Aurora, R.; Rose, G. D. Helix capping. *Protein Sci.* **1998**, *7*, 21-38.

(36) Ramelot, T. A.; Gentile, L. N.; Nicholson, L. K. Transient structure of the amyloid precursor protein cytoplasmic tail indicates preordering of structure for binding to cytosolic factors. *Biochemistry* **2000**, *39*, 2714-2725.

(37) Ramelot, T. A.; Nicholson, L. K. Phosphorylation-induced structural changes in the amyloid precursor protein cytoplasmic tail detected by NMR. *J. Mol. Biol.* **2001**, *307*, 871-884.

(38) Brown, A. M.; Zondlo, N. J. A Propensity Scale for Type II Polyproline Helices (PPII): Aromatic Amino Acids in Proline-Rich Sequences Strongly Disfavor PPII Due to Proline-Aromatic Interactions. *Biochemistry* **2012**, *51*, 5041-5051.

(39) Rucker, A. L.; Pager, C. T.; Campbell, M. N.; Qualls, J. E.; Creamer, T. P. Host-Guest Scale of Left-Handed Polyproline II Helix Formation. *Proteins* **2003**, *53*, 68-75.

(40) Shi, Z.; Chen, K.; Liu, Z.; Ng, A.; Bracken, W. C.; Kallenbach, N. R. Polyproline II propensities from GGXGG peptides reveal an anticorrelation with b-sheet scales. *Proc. Natl. Acad. Sci. USA* **2005**, *102*, 17964-17968.

(41) Woody, R. W. Circular Dichroism Spectrum of Peptides in the Poly(Pro)II Conformation. *J. Am. Chem. Soc.* **2009**, *131*, 8234-8245.

(42) Whittington, S. J.; Chellgren, B. W.; Hermann, V. M.; Creamer, T. P. Urea promotes polyproline II helix formation: Implications for protein denatured states. *Biochemistry* **2005**, *44*, 6269-6275.

(43) Elam, W. A.; Schrank, T. P.; Campagnolo, A. J.; Hilser, V. J. Temperature and Urea Have Opposing Impacts on Polyproline II Conformational Bias. *Biochemistry* **2013**, *52*, 949-958.

(44) Thorsness, P. E.; Koshland, D. E. Inactivation of Isocitrate Dehydrogenase by Phosphorylation Is Mediated by the Negative Charge of the Phosphate. *J. Biol. Chem.* **1987**, *262*, 10422-10425.

(45) Dean, A. M.; Koshland, D. E. Electrostatic and Steric Contributions to Regulation at the Active-Site of Isocitrate Dehydrogenase. *Science* **1990**, *249*, 1044-1046.

(46) Vuister, G. W.; Bax, A. Quantitative J Correlation: A New Approach for Measuring Homonuclear Three-Bond J_{HNHa} Coupling Constants in ^{15}N-enriched Proteins. *J. Am. Chem. Soc.* **1993**, *115*, 7772-7777.

(47) Theillet, F. X.; Smet-Nocca, C.; Liokatis, S.; Thongwichian, R.; Kosten, J.; Yoon, M. K.; Kriwacki, R. W.; Landrieu, I.; Lippens, G.; Selenko, P. Cell signaling, post-translational protein modifications and NMR spectroscopy. *J. Biomol. NMR* **2012**, *54*, 217-236.

(48) Gandhi, N. S.; Landrieu, I.; Byrne, C.; Kukic, P.; Amniai, L.; Cantrelle, F. X.; Wieruszeski, J. M.; Mancera, R. L.; Jacquot, Y.; Lippens, G. A Phosphorylation-Induced Turn Defines the Alzheimer's Disease AT8 Antibody Epitope on the Tau Protein. *Angew. Chem., Int. Ed.* **2015**, *54*, 6819-6823.

(49) Conibear, A. C.; Rosengren, K. J.; Becker, C. F. W.; Kaehlig, H. Random coil shifts of posttranslationally modified amino acids. *J. Biomol. NMR* **2019**, *73*, 587-599.

(50) Cierpicki, T.; Otlewski, J. Amide proton temperature coefficients as hydrogen bond indicators in proteins. *J. Biomol. NMR* **2001**, *21*, 249-261.

(51) Spera, S.; Bax, A. Empirical correlation between protein backbone conformation and Ca and Cb ^{13}C nuclear magnetic resonance chemical shifts. *J. Am. Chem. Soc.* **1991**, *113*, 5490-5492.

(52) Wishart, D. S.; Sykes, B. D.; Richards, F. M. The chemical shift index: a fast and simple method for the assignment of protein secondary structure through NMR spectroscopy. *Biochemistry* **1992**, *31*, 1647-1651.

(53) Wishart, D. S.; Sykes, B. D. The C-13 Chemical Shift Index - A Simple Method for the Identification of Protein Secondary Structure Using C-13 Chemical-Shift Data. *J. Biomol. NMR* **1994**, *4*, 171-180.

(54) Yang, J.; Ten Eyck, L. F.; Xuong, N.-H.; Taylor, S. S. Crystal Structure of a cAMP-dependent Protein Kinase Mutant at 1.26 Å: New Insights into the Catalytic Mechanism. *J. Mol. Biol.* **2004**, *336*, 473-487.

(55) Pérez, C.; Lühr, F.; Rüterjans, H.; Schmidt, J. M. Self-Consistent Karplus Parametrization of 3J Couplings Depending on the Polypeptide Side-Chain Torsion x1. *J. Am. Chem. Soc.* **2001**, *123*, 7081-7093.

(56) Schmidt, J. M. Asymmetric Karplus Curves for the Protein Side-Chain 3J couplings. *J. Biomol. NMR* **2007**, *37*, 287-301.

(57) Lankhorst, P. P.; Haasnoot, C. A. G.; Erkelens, C.; Altona, C. Nucleic Acid Constituents. 36. C-13 NMR in Conformational-Analysis of Nucleic-Acid Fragments. 2. A Reparametrization of the Karplus Equation for Vicinal NMR Coupling-Constants in CCOP and HCOP Fragments. *J. Biomol. Struct. Dynam.* **1984**, *1*, 1387-1405.

(58) Hinderaker, M. P.; Raines, R. T. An electronic effect on protein structure. *Protein Sci.* **2003**, *12*, 1188-1194.

(59) Corzana, F.; Busto, J. H.; Jimenez-Oses, G.; de Luis, M. G.; Asensio, J. L.; Jimenez-Barbero, J.; Peregrina, J. M.; Avenoza, A. Serine versus threonine glycosylation: The methyl group causes a drastic alteration on the carbohydrate orientation and on the surrounding water shell. *J. Am. Chem. Soc.* **2007**, *129*, 9458-9467.

(60) Martínez-Sáez, N.; Castro-López, J.; Valero-González, J.; Madariaga, D.; Compañón, I.; Somovilla, V. J.; Salvadó, M.; Asensio, J. L.; Jiménez-Barbero, J.; Avenoza, A.; Busto, J. H.; Bernardes, G. J. L.; Peregrina, J. M.; Hurtado-Guerrero, R.; Corzana, F. Deciphering the Non-Equivalence of Serine and Threonine O -Glycosylation Points: Implications for Molecular Recognition of the Tn Antigen by an anti-MUC1 Antibody. *Angew. Chem. Int. Ed.* **2015**, *54*, 9830-9834.

(61) Barchi, J. J.; Strain, C. N. The effect of a methyl group on structure and function: Serine vs. threonine glycosylation and phosphorylation. *Front. Mol. Biosci.* **2023**, *10*, 1117850.

(62) Wolfe, S.; Pinto, B. M.; Varma, V.; Leung, R. Y. N. The Perlin Effect - Bond Lengths, Bond Strengths, and the Origins of Stereoelectronic Effects Upon One-Bond C-H Coupling-Constants. *Can. J. Chem.* **1990**, *68*, 1051-1062.

(63) Juaristi, E.; Cuevas, G. Manifestations of stereoelectronic interactions in (1)J(C-H) one-bond coupling constants. *Acc. Chem. Res.* **2007**, *40*, 961-970.

(64) Alabugin, I. V.; Gomes, G. D.; Abdo, M. A. Hyperconjugation. *WIREs Comput. Mol. Sci.* **2019**, *9*, e1389.

(65) Bretscher, L. E.; Jenkins, C. L.; Taylor, K. M.; DeRider, M. L.; Raines, R. T. Conformational Stability of Collagen Relies on a Stereoelectronic Effect. *J. Am. Chem. Soc.* **2001**, *123*, 777-778.

(66) Hodges, J. A.; Raines, R. T. Energetics of an n->pi* interaction that impacts protein structure. *Org. Lett.* **2006**, *8*, 4695-4697.

(67) Bartlett, G. J.; Choudhary, A.; Raines, R. T.; Woolfson, D. N. n->pi* interactions in proteins. *Nat. Chem. Biol.* **2010**, *6*, 615-620.

(68) Shoulders, M. D.; Satyshur, K. A.; Forest, K. T.; Raines, R. T. Stereoelectronic and steric effects in side chains preorganize a protein main chain. *Proc. Natl. Acad. Sci. U.S.A.* **2010**, *107*, 559-564.

(69) Newberry, R. W.; VanVeller, B.; Guzei, I. A.; Raines, R. T. n ->pi* Interactions of Amides and Thioamides: Implications for Protein Stability. *J. Am. Chem. Soc.* **2013**, *135*, 7843-7846.

(70) Newberry, R. W.; Raines, R. T. The n->pi* interaction. *Acc. Chem. Res.* **2017**, *50*, 1838-1846.

(71) Schutkowski, M.; Bernhardt, A.; Zhou, X. Z.; Shen, M. H.; Reimer, U.; Rahfeld, J. U.; Lu, K. P.; Fischer, G. Role of phosphorylation in determining the backbone dynamics of the serine/threonine-proline motif and Pin1 substrate recognition. *Biochemistry* **1998**, *37*, 5566-5575.

(72) Yeates, T. O.; Kent, S. B. H.: Racemic Protein Crystallography. In *Ann. Rev. Biophysics*; Annual Review of Biophysics, 2012; Vol. 41; pp 41-61.

(73) Gilli, G.; Gilli, P.: *The Nature of the Hydrogen Bond: Outline of a Comprehensive Hydrogen Bond Theory*; Oxford University Press: New York, 2009.

(74) Zondlo, N. J. Solvation stabilizes intercarbonyl n→π* interactions and polyproline II helix. *Phys. Chem. Chem. Phys.* **2022**, *24*, 13571-13586.

(75) Reed, A. E.; Curtiss, L. A.; Weinhold, F. Intermolecular Interactions from a Natural Bond Orbital, Donor-Acceptor Viewpoint. *Chem. Rev.* **1988**, *88*, 899-926.

(76) DeRider, M. L.; Wilkens, S. J.; Waddell, M. J.; Bretscher, L. E.; Weinhold, F.; Raines, R. T.; Markley, J. L. Collagen Stability: Insights from NMR Spectroscopic and Hybrid Density Functional Computational Investigations of the Effect of Electronegative Substituents on Prolyl Ring Conformations. *J. Am. Chem. Soc.* **2002**, *124*, 2497-2505.

(77) Yonemoto, W.; McGlone, M. L.; Grant, B.; Taylor, S. S. Autophosphorylation of the catalytic subunit of cAMP-dependent protein kinase in Escherichia coli. *Protein Eng.* **1997**, *10*, 915-925.

(78) Steichen, J. M.; Kuchinskas, M.; Keshwani, M. M.; Yang, J.; Adams, J. A.; Taylor, S. S. Structural Basis for the Regulation of Protein Kinase A by Activation Loop Phosphorylation. *J. Biol. Chem.* **2012**, *287*, 14672-14680.

(79) Lee, C. W.; Ferreon, J. C.; Ferreon, A. C. M.; Arai, M.; Wright, P. E. Graded enhancement of p53 binding to CREB-binding protein (CBP) by multisite phosphorylation. *Proc. Natl. Acad. Sci. USA* **2010**, *107*, 19290-19295.

(80) Bah, A.; Vernon, R. M.; Siddiqui, Z.; Krzeminski, M.; Muhandiram, R.; Zhao, C.; Sonenberg, N.; Kay, L. E.; Forman-Kay, J. D. Folding of an intrinsically disordered protein by phosphorylation as a regulatory switch. *Nature* **2015**, *519*, 106-109.

(81) Lippens, G.; Landrieu, I.; Smet, C.; Huvent, I.; Gandhi, N. S.; Gigant, B.; Despres, C.; Qi, H. L.; Lopez, J. NMR Meets Tau: Insights into Its Function and Pathology. *Biomolecules* **2016**, *6*, 28.

(82) Neira, J. L.; Rizzuti, B.; Jimenez-Alesanco, A.; Palomino-Schatzlein, M.; Abian, O.; Velazquez-Campoy, A.; Iovanna, J. L. A Phosphorylation-Induced Switch in the Nuclear

Localization Sequence of the Intrinsically Disordered NUPR1 Hampers Binding to Importin. *Biomolecules* **2020**, *10*, 1313.

(83) Chaves-Arquero, B.; Perez-Canadillas, J. M.; Jimenez, M. A. Effect of Phosphorylation on the Structural Behaviour of Peptides Derived from the Intrinsically Disordered C-Terminal Domain of Histone H1.0. *Chem. Eur. J.* **2020**, *26*, 5970-5981.

(84) Cantrelle, F. X.; Loyens, A.; Trivelli, X.; Reimann, O.; Despres, C.; Gandhi, N. S.; Hackenberger, C. P. R.; Landrieu, I.; Smet-Nocca, C. Phosphorylation and O-GlcNAcylation of the PHF-1 Epitope of Tau Protein Induce Local Conformational Changes of the C-Terminus and Modulate Tau Self-Assembly Into Fibrillar Aggregates. *Front. Mol. Neurosci.* **2021**, *14*, 661368.

(85) Kim, S. Y.; Harvey, C. M.; Giese, J.; Lassowskat, I.; Singh, V.; Cavanagh, A. P.; Spalding, M. H.; Finkemeier, I.; Ort, D. R.; Huber, S. C. In vivo evidence for a regulatory role of phosphorylation of Arabidopsis Rubisco activase at the Thr78 site. *Proc. Natl. Acad. Sci. U.S.A.* **2019**, *116*, 18723-18731.

(86) Ferreon, J. C.; Lee, C. W.; Arai, M.; Martinez-Yamout, M. A.; Dyson, H. J.; Wright, P. E. Cooperative regulation of p53 by modulation of ternary complex formation with CBP/p300 and HDM2. *Proc. Natl. Acad. Sci. USA* **2009**, *106*, 6591-6596.

(87) Bozoky, Z.; Krzeminski, M.; Muhandiram, R.; Birtley, J. R.; Al-Zahrani, A.; Thomas, P. J.; Frizzell, R. A.; Ford, R. C.; Forman-Kay, J. D. Regulatory R region of the CFTR chloride channel is a dynamic integrator of phospho-dependent intra- and intermolecular interactions. *Proc. Natl. Acad. Sci. U.S.A.* **2013**, *110*, E4427-E4436.

(88) Shackelford, D. B.; Shaw, R. J. The LKB1-AMPK pathway: metabolism and growth control in tumour suppression. *Nat. Rev. Cancer* **2009**, *9*, 563-575.

(89) Bremmer, S. C.; Hall, H.; Martinez, J. S.; Eissler, C. L.; Hinrichsen, T. H.; Rossie, S.; Parker, L. L.; Hall, M. C.; Charbonneau, H. Cdc14 Phosphatases Preferentially Dephosphorylate a Subset of Cyclin-dependent kinase (Cdk) Sites Containing Phosphoserine. *J. Biol. Chem.* **2012**, *287*, 1662-1669.

(90) Rani, L.; Majllajosyula, S. S. Phosphorylation versus O-GlcNAcylation: Computational Insights into the Differential Influences of the Two Competitive Post-Translational Modifications. *J. Phys. Chem. B* **2017**, *121*, 10618-10638.

(91) Shen, T.; Wong, C. F.; McCammon, J. A. Atomistic Brownian Dynamics Simulation of Peptide Phosphorylation. *J. Am. Chem. Soc.* **2001**, *123*, 9107-9111.

(92) Hamelberg, D.; Shen, T.; McCammon, J. A. Phosphorylation effects on cis/trans isomerization and the backbone conformation of serine-proline motifs: accelerated molecular dynamics analysis. *J. Am. Chem. Soc.* **2005**, *127*, 1969-1974.

(93) Wong, S. E.; Bernacki, K.; Jacobson, M. Competition between intramolecular hydrogen bonds and solvation in phosphorylated peptides: simulations with explicit and implicit solvent. *J. Phys. Chem. B* **2005**, *109*, 5249-5258.

(94) Latzer, J.; Shen, T.; Wolynes, P. G. Conformational switching upon phosphorylation: A predictive framework based on energy landscape principles. *Biochemistry* **2008**, *47*, 2110-2122.

(95) Vymetal, J.; Juraskova, V.; Vondrasek, J. AMBER and CHARMM Force Fields Inconsistently Portray the Microscopic Details of Phosphorylation. *J. Chem. Theory Comput.* **2019**, *15*, 665-679.

(96) Iakoucheva, L. M.; Radivojac, P.; Brown, C. J.; O'Connor, T. R.; Sikes, J. G.; Obradovic, Z.; Dunker, A. K. The importance of intrinsic disorder for protein phosphorylation. *Nucleic Acids Res.* **2004**, *32*, 1037-1049.

(97) Elam, W. A.; Schrank, T. P.; Campagnolo, A. J.; Hilser, V. J. Evolutionary conservation of the polyproline II conformation surrounding intrinsically disordered phosphorylation sites. *Protein Sci.* **2013**, *22*, 405-417.

(98) Wang, G.; Dunbrack, R. L. PISCES: a protein sequence culling server. *Bioinformatics* **2003**, *19*, 1589-1591.

(99) Sheldrick, G. M. A short history of SHELX. *Acta Cryst.* **2008**, *A64*, 112-122.

(100) Spek, A. L. Structural validation in chemical crystallography. *Acta. Cryst.* **2009**, *D65*, 148-155.

(101) Frisch, M. J.; Trucks, G. W.; Schlegel, H. B.; Scuseria, G. E.; Robb, M. A.; Cheeseman, J. R.; Scalmani, G.; Barone, V.; Mennucci, B.; Petersson, G. A.; Nakatsuji, H.; Caricato, M.; Li, X.; Hratchian, H. P.; Izmaylov, A. F.; Bloino, J.; Zheng, G.; Sonnenberg, J. L.; Hada, M.; Ehara, M.; Toyota, K.; Fukuda, R.; Hasegawa, J.; Ishida, M.; Nakajima, T.; Honda, Y.; Kitao, O.; Nakai, H.; Vreven, T.; Montgomery, J., J. A.; Peralta, J. E.; Ogliaro, F.; Bearpark, M.; Heyd, J. J.; Brothers, E.; Kudin, K. N.; Staroverov, V. N.; Keith, T.; Kobayashi, R.; Normand, J.; Raghavachari, K.; Rendell, A.; Burant, J. C.; Iyengar, S. S.; Tomasi, J.; Cossi, M.; Rega, N.; Millam, J. M.; Klene, M.; Knox, J. E.; Cross, J. B.; Bakken, V.; Adamo, C.; Jaramillo, J.; Gomperts, R.; Stratmann, R. E.; Yazyev, O.; Austin, A. J.; Cammi, R.; Pomelli, C.; Ochterski, J. W.; Martin, R. L.; Morokuma, K.; Zakrzewski, V. G.; Voth, G. A.; Salvador, P.; Dannenberg, J. J.; Dapprich, S.; Daniels, A. D.; Farkas, O.; Foresman, J. B.; Ortiz, J. V.; Cioslowski, J.; Fox, D. J.: Gaussian 09, Revision D.01. Gaussian, Inc.: Wallingford, CT, 2013.

(102) Wenzell, N. A.; Ganguly, H. K.; Pandey, A. K.; Bhatt, M. R.; Yap, G. P. A.; Zondlo, N. J. Electronic and steric control of n→π* interactions via N-capping: stabilization of the α-helix conformation without a hydrogen bond. *ChemBioChem* **2019**, *20*, 963-967.

(103) Zhao, Y.; Truhlar, D. G. The M06 suite of density functionals for main group thermochemistry, thermochemical kinetics, noncovalent interactions, excited states, and transition elements: two new functionals and systematic testing of four M06-class functionals and 12 other functionals. *Theor. Chem. Acc.* **2008**, *120*, 215-241.

(104) Raghavachari, K.; Binkley, J. S.; Seeger, R.; Pople, J. A. Self-Consistent Molecular Orbital Methods. 20. Basis sets for correlated wave functions. *J. Chem. Phys.* **1980**, *72*, 650-654.

(105) Tomasi, J.; Mennucci, B.; Cances, E. The IEF version of the PCM solvation method: an overview of a new method addressed to study molecular solutes at the QM ab initio level. *J. Mol. Struct. THEOCHEM* **1999**, *464*, 211-226.

(106) Dunning, T. H. Gaussian-Basis Sets for Use in Correlated Molecular Calculations. 1. The Atoms Boron through Neon and Hydrogen. *J. Chem. Phys.* **1989**, *90*, 1007-1023.

(107) Glendening, E. D.; Landis, C. R.; Weinhold, F. NBO 6.0: Natural bond orbital analysis program. *J. Computational Chem.* **2013**, *34*, 1429-1437.

Graphical Table of Contents entry